Ore Geology Reviews 78 (2016) 120–137

Contents lists available at ScienceDirect

Ore Geology Reviews

journal homepage: www.elsevier.com/locate/oregeorev

Geochronological and petrogeochemical constraints on the skarn deposits in Tongshanling ore district, southern Hunan Province: Implications for Jurassic Cu and W metallogenic events in South China

Panlao Zhao [a], Shunda Yuan [a,*], Jingwen Mao [a], M. Santosh [b,c], Chao Li [d], Kejun Hou [a]

[a] MLR Key Laboratory of Metallogeny and Mineral Assessment, Institute of Mineral Resources, Chinese Academy of Geological Sciences, Beijing 100037, China
[b] Centre for Tectonics, Resources and Exploration, Department of Earth Sciences, School of Physical Sciences, University of Adelaide, SA 5005, Australia
[c] School of Earth Sciences and Resources, China University of Geosciences, 100083 Beijing, China
[d] National Research Center for Geoanalysis, Beijing 100037, China

ARTICLE INFO

Article history:
Received 9 December 2015
Received in revised form 7 March 2016
Accepted 10 March 2016
Available online 23 March 2016

Keywords:
Zircon U–Pb geochronology
Re-Os isotope systematics
Petrogenesis
Skarn mineralization
South China

ABSTRACT

Southern Hunan Province, South China, is located in the central part of the Qin–Hang metallogenic belt and is characterized by abundant Cu–Pb–Zn and W–Sn polymetallic ore deposits. The Cu–Pb–Zn deposits are associated with Jurassic granodiorite porphyries whereas the W–Sn deposits occur within Jurassic granite porphyries. Here we present geochronologic and geochemical data for the Tongshanling Cu–(Mo)–Pb–Zn deposit and the Weijia W deposit in the district of Tongshanling, southern Hunan. Zircon U–Pb dating and molybdenite Re–Os geochronology indicate that the emplacement of the Tongshanling granodiorite porphyry and the associated Cu mineralization occurred at 162–160 Ma, slightly earlier than the formation of the Xianglinpu granite porphyry and associated W mineralization at 159–158 Ma. The Tongshanling granodiorite is high-K calc-alkaline, weakly peraluminous, and weakly fractionated with zircon $\varepsilon_{Hf}(t)$ values of −15.1 to −5.6. In contrast, the Xianglinpu granite is alkaline, peraluminous, and highly fractionated, with $\varepsilon_{Hf}(t)$ values of −9.5 to 0.9. Our data indicate that the Tongshanling granodiorite is relatively oxidized and was formed by the partial melting of Paleoproterozoic crustal material with inputs of mafic magma which was derived from a subduction-modified lithospheric mantle. In contrast, the Xianglinpu granite porphyry is relatively reduced and was formed by direct interaction between the crust and asthenospheric mantle. The difference in magma generation and tectonics is considered to have resulted in the different types of mineralization associated with these two intrusive bodies.

1. Introduction

The southern Hunan Province in South China occurs within the tectonic boundary between the Yangtze and Cathaysian blocks, and also marks the zone intersection between the Nanling W–Sn metallogenic province and the Qin–Hang (Qinzhou Bay to Hangzhou Bay) Cu polymetallic belt (Fig. 1). Since the Mesozoic, this region has experienced complex tectonic activity and widespread magmatism (Faure and Ishida, 1990; Maruyama et al., 1997; Zhou et al., 2006). These events contributed to the emplacement of large volumes of granitoids and the formation of numerous associated ore deposits, making this area an important region for large-scale Mesozoic metallogenesis in eastern China (Hua and Mao, 1999; Mao et al., 1999a).The ore deposits not only include many large-sized, granite-associated W–Sn deposits, such as the Shizhuyuan W–Sn–Mo–Bi (Mao and Li, 1995; Mao et al., 1996; Lu et al., 2003), Hongqiling Sn–W–Pb–Zn (Yuan et al., 2012a), Furong Sn (Mao et al., 2004; Peng et al., 2007; Yuan et al., 2008a, 2011), Xintianling W–Mo (Yuan et al., 2012b), and Xianghualing Sn–Pb–Zn deposits (Yuan et al., 2007, 2008b, 2008c), but also several granodiorite-related Cu–Pb–Zn polymetallic deposits, such as the Tongshanling Cu–Pb–Zn (Wang et al., 2001), Baoshan Cu–Pb–Zn (Lu et al., 2006; Mi et al., 2014), and Shuikoushan Pb–Zn–Cu deposits (Ma et al., 2006; Huang et al., 2015). The petrogenesis of the granitic rocks, the spatial–temporal distribution of the granitic plutons and associated ore deposits, and the corresponding geodynamic setting, have all received considerable attention (Hua et al., 2005, 2010; Li and Li, 2007; Chen et al., 2008; Mao et al., 2008, 2011b, 2013). However, the formation of two distinct metallogenic assemblages, the W–Sn and Cu–Pb–Zn deposits in the same region remains an enigma. To answer this question, systematic investigations on the geochronology and petrogenesis of the host rocks associated with the mineralization are needed to define the characteristics and nature of their sources.

The Tongshanling deposit is the largest Cu-dominant Cu–(Mo)–Pb–Zn polymetallic deposit in southern Hunan Province. It has total combined Cu, Pb, and Zn reserves of 2.5×10^6 t (Ding et al., 2015). As a representative Cu polymetallic mineralization of this area, the Tongshanling deposit is characterized by a series of granodiorite-related skarn Cu–(Mo)–Pb–Zn deposits, such as those in the Tongshanling Cu–Pb–

* Corresponding author.
E-mail address: shundayuan@cags.ac.cn (S. Yuan).

http://dx.doi.org/10.1016/j.oregeorev.2016.03.004
0169-1368/

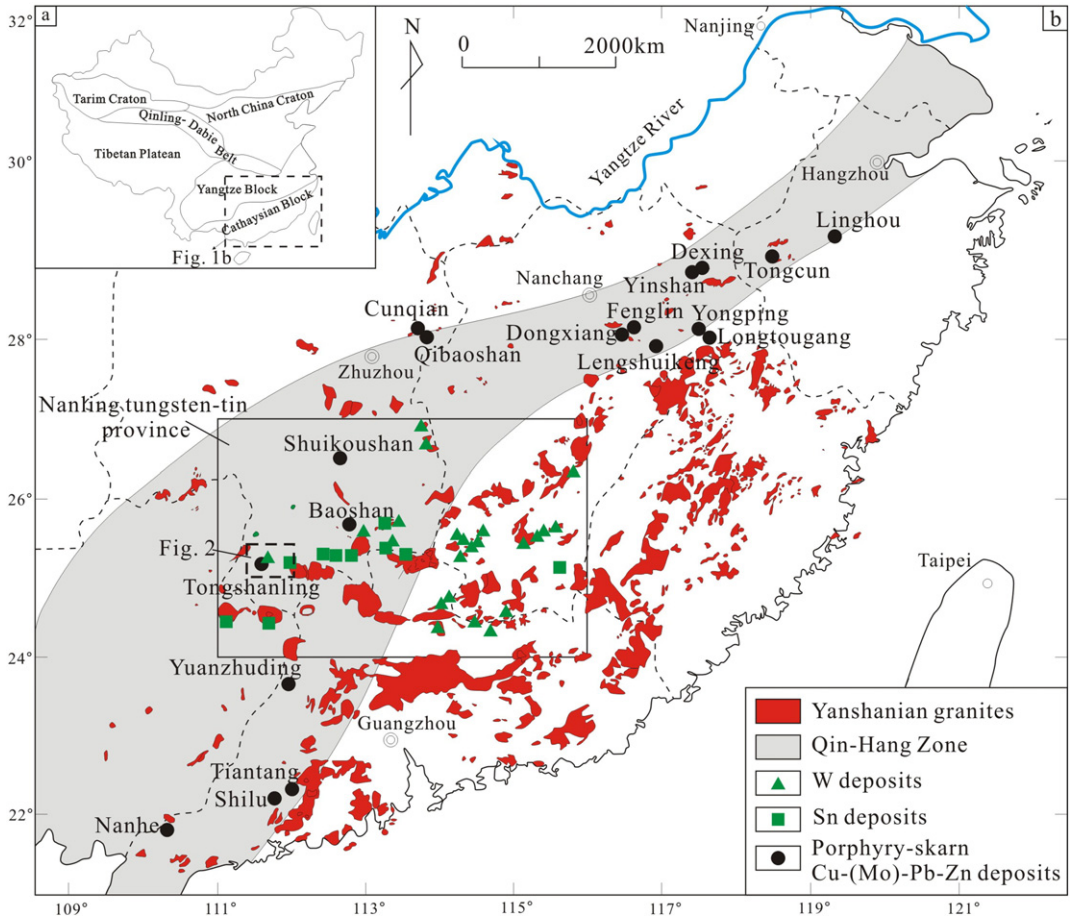

Fig. 1. (a) Sketch tectonic map of China. (b) Simplified geological mapping showing the distribution of Yanshanian granitoids within South China. Also shown are the Cu polymetallic deposits in the Qin–Hang belt and the W–Sn deposits in the Nanling district.
Modified from Zhou et al. (2006) and Mao et al. (2013).

Zn–Ag, Antangling Pb–Zn, Yulong Mo, and Qiaotoupu Pb–Zn mines. The giant skarn-type Weijia W deposit (0.26 Mt of WO_3) was recently discovered ~15 km northeast of the Tongshanling deposit (Li et al., 2012; Yang et al., 2012), and is spatially associated with the Xianglinpu granite porphyry. Previous studies have reported a large range of zircon U–Pb ages for the Tongshanling granodiorite (181–149 Ma; Wang et al., 2001; Wei et al., 2007; Jiang et al., 2009; Quan et al., 2013), with no reliable constraint on the timing of its emplacement. Moreover, the available geochronologic data were also scarce to constrain the timing of the polymetallic Cu mineralization. With respect to the newly discovered Weijia giant W deposit, little is known about the age of mineralization or the petrogenesis of the ore-related granite.

In this paper, we present the results of new whole-rock geochemistry, zircon U–Pb dating and Hf isotope analyses for these ore-related granitic rocks. In addition, molybdenite Re–Os isotope data are provided to constrain the timing of mineralization in the Tongshanling and Weijia deposits. Combined with data from the literature, our new results constrain the timing of mineralization, as well as the sources of the two contrasting types of granitic rock that formed the studied mineralizations. The characteristics of the differing sources for these two types of granitic rock were probably the main controls on the contrasting types of mineralization in the Tongshanling district.

2. Geologic setting

The South China Block is bound by the Qinling–Dabie orogenic belt to the north and by the Indochina and Tibetan blocks to the southwest and west, respectively (Fig. 1a). This major crustal block was formed in the Neoproterozoic by the amalgamation of the Yangtze Block (to the northwest) and the Cathaysia Block (to the southeast) (Chen and Jahn, 1998; Li et al., 2002; Zhou et al., 2002; Yao et al., 2013; Zhang et al., 2013b), and subsequently underwent several periods of rifting and suturing (Shu et al., 2008). The Qin–Hang Belt marks boundary along which the Neoproterozoic amalgamation took place (Shu et al., 2008). The belt is 2000 km long and 100–150 km wide, and it extends from Qinzhou Bay in Guangxi Province, through eastern Hunan and Central Jiangxi provinces, to Hangzhou Bay in Zhejiang Province. The belt is an important Cu–Pb–Zn polymetallic metallogenic zone in southeastern China (Fig.1b; Mao et al., 2010, 2011a, c; Zhou et al., 2012) and is marked by extensive volumes of Jurassic porphyry-skarn Cu polymetallic deposits. The Tongshanling district is located in the central section of the Qin–Hang Belt, and it overlaps with the western part of the Nanling W–Sn province (Fig. 1b).

The basement in the Tongshanling area consists mainly of Cambrian–Ordovician neritic clastic rocks, chert, and carbonate rocks, which are unconformably overlain by Devonian–Triassic neritic carbonates that are intercalated with littoral clastic rocks and Cretaceous terrestrial clastic rocks (Fig. 2). The tectonic framework of this area is controlled mainly by three fault systems that trend approximately NE–SW, NW–SE, and E–W. Among these, the most important are the Shuikoushan–Tongshanling and Tongshanling–Jiuyishan faults as well as the Huaihua–Daoxian basement fault. Together, they control the spatial distribution of granites and associated ore deposits in this area. A number of Mesozoic granite intrusions, diorite–granodiorite intrusions, and multiple types of polymetallic deposits are distributed in this region. The granodiorite intrusions, as exemplified by the examples at Baoshan, Tongshanling, and Shuikoushan,

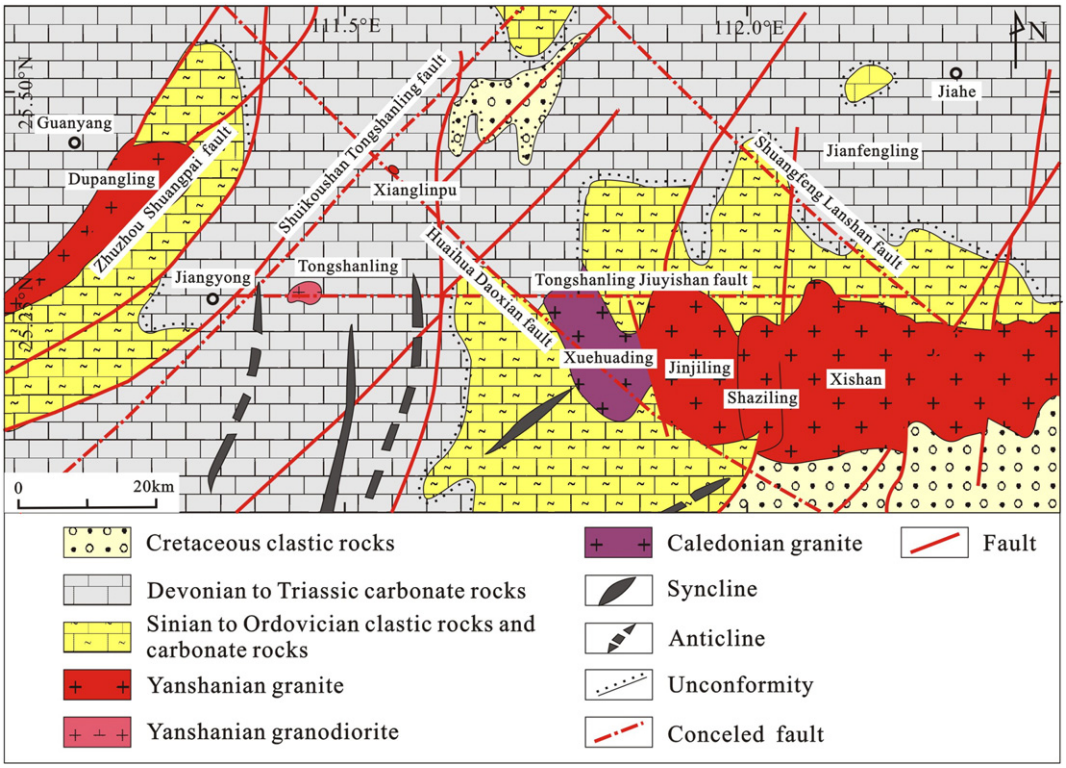

Fig. 2. Simplified geological map of the Tongshanling district, southern Hunan Province. Modified from Li et al. (2012)).

are small in volume, and are associated with skarn type Cu–Pb–Zn mineralization. Granites in the area include the Qitianling, Qianlishan, Xianglinpu, Jinjiling, and Xishan plutons, and the plutons are generally oval in shape and associated with skarn, greisen, granite, and quartz vein-type Sn–W mineralization (Peng et al., 2008). Coeval mafic rocks are scarce, but those such as the Ningyuan alkaline basalts (175 Ma; Li et al., 2004) and Daoxian high-Mg low-Ti basalts (150 Ma; Li et al., 2004) show a close spatial and temporal relationship with the granites.

3. Ore deposit geology

3.1. Geology of the Tongshanling deposit

The Tongshanling Cu–(Mo)–Pb–Zn deposit is located about 10 km east of Jiangyong County in southern Hunan Province. A brief description of the geological features of this region is given in the following sections.

3.1.1. Stratigraphy

The local geology around the Tongshanling deposit is relatively complex and dominated by Devonian, Carboniferous, Permian, and Jurassic sedimentary rocks, most of which are limestone and dolomite (Fig. 3). The Shidengzi Formation is exposed in the northern part of the ore district and consists of gray thick-layered limestones with chert nodules and medium-layered micrites with dolomitic limestones and argillaceous limestones. The Tianeping Formation, in the southern part of the area, is composed of black medium-layered silty mudstones, gray calcilutites, and thin-layered argillaceous limestones with a total thickness of >350 m. The Malanbian Formation, in the southern and western parts of the area, is 200 m thick and consists of dark-gray medium- to thick-layered micrites intercalated with dolomite. The Qiziqiao Formation is 570 m thick and consists mainly of limestone and dolomite. Limestones of the Shidengzi and Qiziqiao Formation are the main host of the Tongshanling Cu polymetallic orebodies.

3.1.2. Structure

Structures in the area are dominated by faults that strike NNE–SSW and nearly E–W(Fig. 3). The NNE–SSW-striking faults are the best developed, and exerted major structural control on the emplacement of the Tongshanling granodiorite and associated mineralization. The Dayuanling anticline, in the eastern part of the area, is the main fold present, and the Tongshanling Cu–Pb–Zn ore deposit was developed on its western limb.

3.1.3. Igneous rocks

The Tongshanling granodiorite was emplaced within Upper Devonian and Lower Carboniferous rocks, and it consists of three nearly W–E-striking stocks with a total surface exposure of ~12 km^2. The main part of the Tongshanling granodiorite is dominated by a porphyritic biotite granodiorite that is closely associated with the mineralization. The granodiorite porphyry is gray in color and exhibits a massive structure and porphyritic texture (Fig. 6a). It is dominated by 0.6–1.2 cm phenocrysts (~35%–45% of the rock mass) of plagioclase (~60% of the total phenocrysts), K-feldspar (~14%), quartz (~20%), and biotite (~7%), set in a fine-grained groundmass (~65%–55% of the rock mass) of plagioclase (~45% of the matrix), quartz (~30%), K-feldspar (~15%), biotite (~5%) and amphibole (~3%) (Fig. 6b). In addition, some felsic dikes in the northeastern part of the area represent a late stage of magmatism, as they cut through the Tongshanling granodiorite and associated ore bodies.

3.1.4. Alteration and mineralization

The Tongshanling Cu polymetallic deposit comprises a series of ore bodies that are distributed around the Tongshanling granodiorite porphyry, and the most important are those being worked in the Tongshanling Cu–Pb–Zn, Antangling Pb–Zn–Ag, Yulong Mo, and

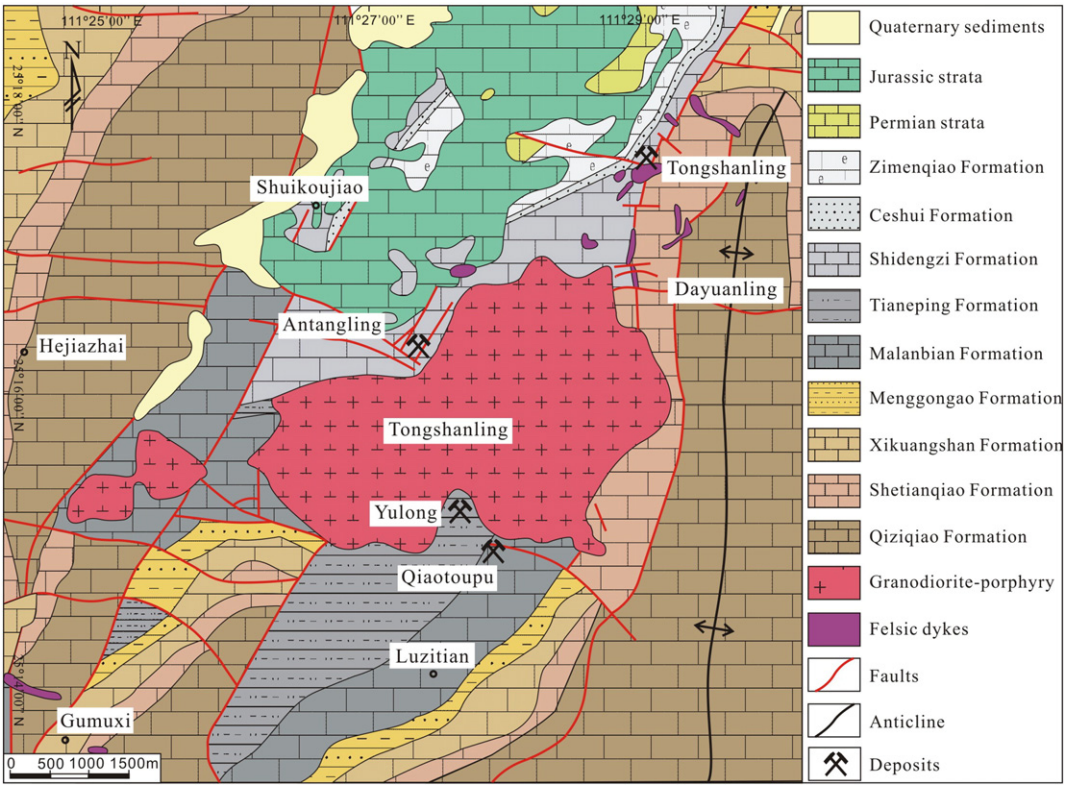

Fig. 3. Simplified geological map of the Tongshanling Cu–(Mo)–Pb–Zn deposit, southern Hunan Province. Modified from Cai et al. (2015).

Qiaotoupu Pb–Zn mines. Mineralization associated with hydrothermal alteration occurs mainly within the contact zone between the granodiorite stocks and the country rock. The mineralization shows pronounced zoning from skarn type, through sulfide-quartz vein type, and finally carbonate-replacement type, from proximal to distal (Fig. 5). Skarn type ores mainly occur in the NNE–SSW-trending contact zone between the intrusion and the Devonian limestone as stratiform, lensoid, and irregular bodies and host the most economically important Cu-Pb-Zn mineralization. Sulfide-quartz vein type ore bodies mainly fill NWW–SEE- and NE–SW-trending fractures. Carbonate-replacement ores are of low economic importance in this area. Based on mineral assemblages, ore textures and vein crosscutting relationships, the mineralization can be divided into prograde, retrograde, and quartz–sulfide vein stages (Fig. 5). The prograde stage of alteration is characterized by the metasomatism of limestone to garnet, diopside, and wollastonite calc-silicate skarn. The retrograde alteration stage is characterized by the replacement of the majority of garnet and diopside by actinolite, epidote, and chlorite, and the deposition of abundant sulfides (mainly chalcopyrite, pyrite, molybdenite, sphalerite, and galena) that form both massive and disseminated ores. The quartz-sulfide vein stage is dominated by the formation of chalcopyrite-pyrite–pyrrhotite–quartz veins and pyrite–sphalerite–galena–quartz veins. These veins form veinlet–disseminated ores with low grade. Molybdenite, intergrown with pyrite, chalcopyrite, sphalerite, and quartz, were formed during the major Cu-Pb-Zn mineralization stage (Figs. 5, 6).

3.2. Geology of the Weijia tungsten deposit

The Weijia ore deposit is located in the northeastern Jiangyong County in southern Hunan Province, 15 km northeast of the Tongshanling copper polymetallic deposit.

3.2.1. Stratigraphy

Sedimentary strata in the Xianglinpu area consist predominantly of the Devonian Qiziqiao, Changlongjie, and Xikuangshan formations (Fig. 4), which form a suite of neritic–littoral carbonate rocks, clastic rocks, and terrestrial clastic rocks. The Qiziqiao Formation, in the central part of the area, is dominated by bioclastic limestones, limestones, and dolomites, and it can be subdivided into three subgroups, with the limestones of the middle part of the Middle Devonian Qiziqiao Formation hosting the tungsten mineralization. The Changlongjie Formation is 50 m thick and consists of gray–black medium- to thick-layered micritic limestones and terrestrial clastic rocks. The Xikuangshan Formation, in the western and southeastern parts of the area, is up to 200 m thick and consists of gray–white thick-layered micritic limestones intercalated with dolomite.

3.2.2. Structure

The Xianglinpu anticlinorium is the main structure in the study area, and it includes the Xianglinpu anticline, the Baigangling syncline, and the Zhuling anticline (Fig. 4). The limestone of the Qiziqiao Formation occurs in the center of the anticlinorium, and the micritic limestones of the Changlongjie and Xikuangshan Formations form the eastern and western limbs, respectively. The Xianglinpu granite and its associated tungsten ore deposit are located within the core and the western flank of the Xianglinpu anticlinorium.

3.2.3. Igneous rocks

The main igneous rock complex in the study area is the Xianglinpu porphyritic granite dike swarm, which is composed of 31 E–W-trending small plutons and dikes, with the largest having a surface exposure of 0.35 km^2 in the central part of the Xianglinpu anticline. The granite porphyry is pink in color, and it exhibits a massive structure and porphyritic texture (Fig. 6c). It is dominated by 0.5–1 mm phenocrysts (~30% of the

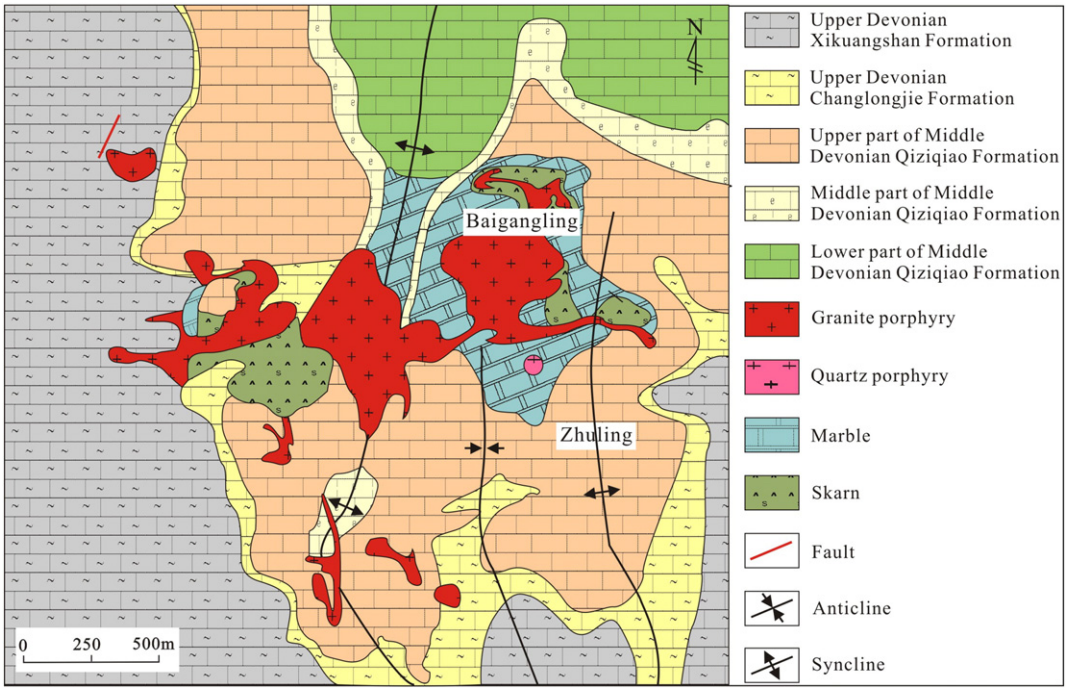

Fig. 4. Simplified geological map of the Weijia W deposit, southern Hunan Province. Modified from Yang et al. (2012).

rock mass) of K-feldspar (~50% of the total phenocrysts), quartz (~35%), and plagioclase (~15%), set in a 0.05–0.1 mm matrix that contains K-feldspar (~45% of the matrix), quartz (~35%), plagioclase (~15%), and biotite (~5%). Some feldspar phenocrysts in the porphyritic granite have been altered to fine-grained sericite (Fig. 6d).

3.2.4. Alteration and mineralization

Field observations and drill-core logging show that the mineralization associated with hydrothermal alteration occurs mainly within the contact zone between the Xianglinpu granite porphyry and the country rock. The alteration is zoned, and from the center outwards it includes greisen, skarn, serpentine, marble, and carbonate alteration. The skarns are by far the most important of these, and they contain economically significant tungsten mineralization. Drilling shows that tungsten-bearing skarns occur in the western part of the area as concealed orebodies at a depth of 500 m below the surface, and the skarns are generally located in impure limestones and dolomites of the Qiziqiao Formation. The largest economic orebody has a thickness of 139.73 m, and the average grade of the ore is 0.18% WO_3. The important ore minerals are scheelite, chalcopyrite, and molybdenite, with minor pyrite, cassiterite,

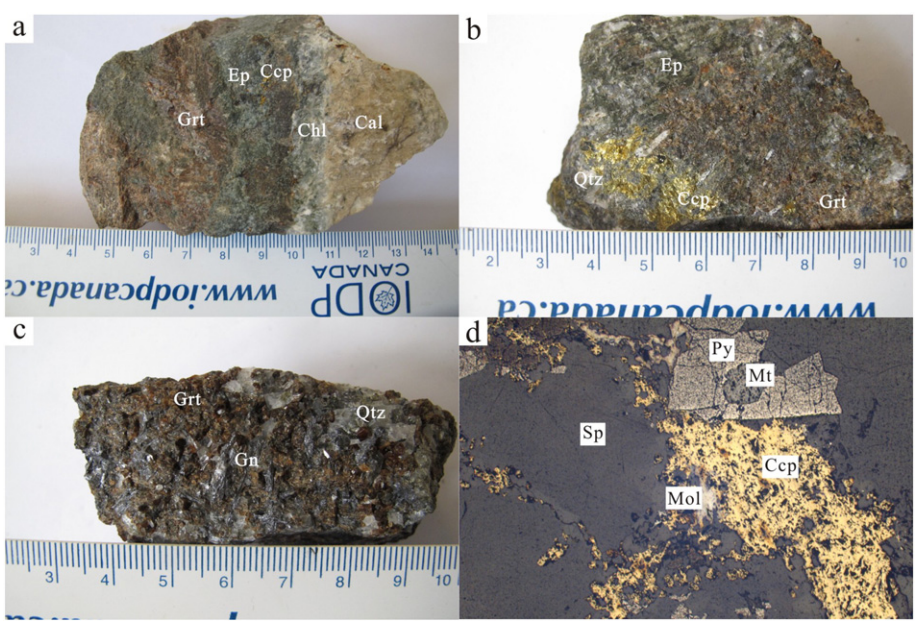

Fig. 5. Photographs of hand specimens and micrographs of molybdenite-bearing ores collected from the Tongshanling Cu–(Mo)–Pb–Zn deposit. (a) Skarn alteration; (b) skarn–type Cu ores; (c) sulfide–quartz vein type Pb ores. (d) Molybdenite associated with pyrite, chalcopyrite, and sphalerite (under reflected light). (Cal: calcite; Ccp: chalcopyrite; Chl: chlorite; Ep: epidote; Gn: galena; Grt: garnet; Mt: magnetite; Qtz: quartz; Sp: sphalerite).

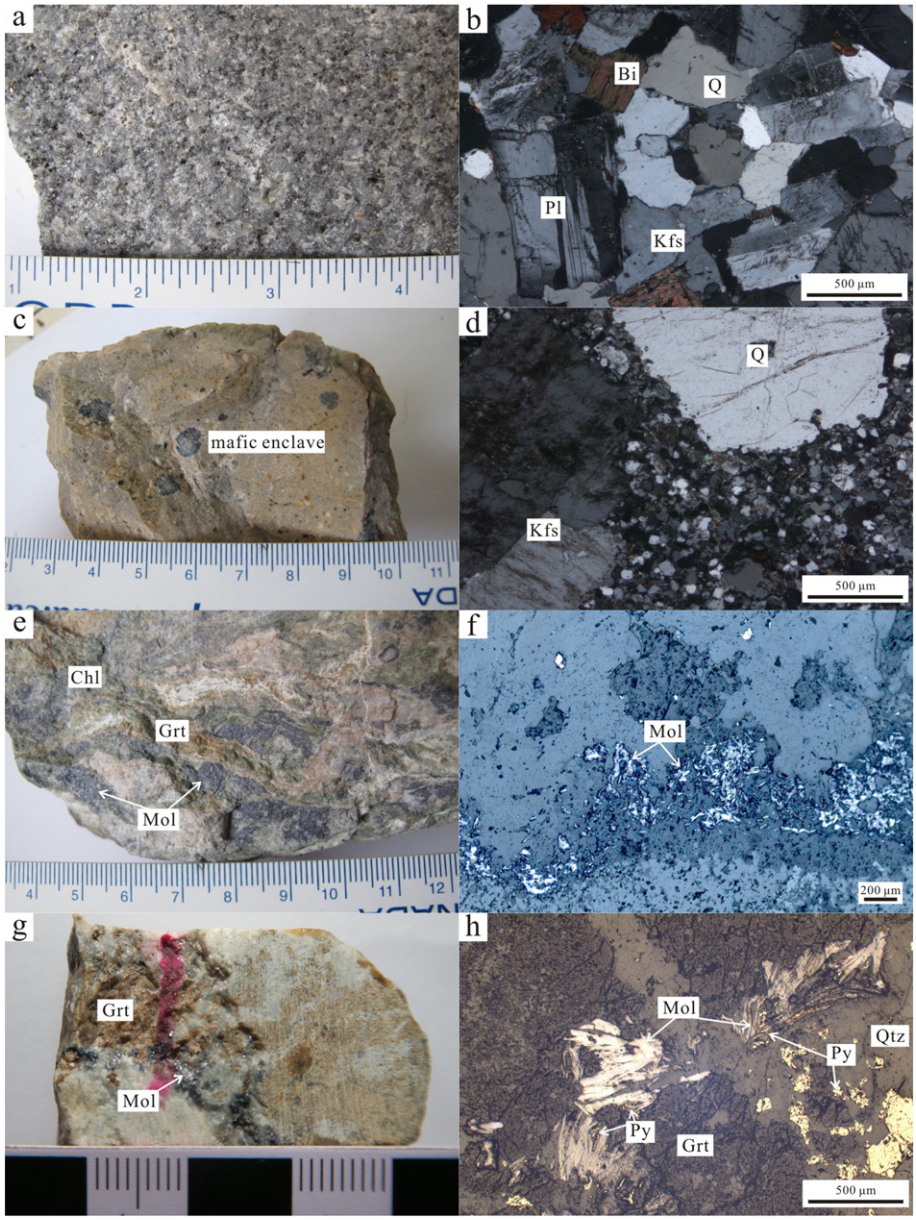

Fig. 6. Samples and photomicrographs of the ore-related granitic rocks and molybdenite for the Tongshanling and Weijia deposits. (Am: amphibole; Bi: biotite; Kfs: K-feldspar; Mol: molybdenite; Pl: plagioclase; Q: quartz; Grt: garnet; Ccp: chalcopyrite).

and sphalerite. The scheelite is typically present as disseminations and veinlets within the skarn.

4. Sampling and analytical methods

4.1. Sampling

Three granodiorite porphyry samples were selected from two mines within the Tongshanling deposit for zircon U–Pb dating and *in situ* zircon Lu–Hf analysis (Fig. 3). Six granodiorite porphyry samples were selected from the Tongshanling mine for major and trace element analysis, and five molybdenite samples were collected from the Yulong mine for Re–Os dating (Fig. 6e, f). The Xianglinpu granite porphyry samples were collected from surface exposures of the Weijia W deposit. These included two samples for *in situ* zircon Hf analysis with zircon U-Pb age of 158 Ma (Zhao et al., 2016), and five for major and trace element analyses (Fig. 4). Four molybdenite samples were collected from skarns within the Weijia tungsten deposit for Re–Os dating (Fig. 6g, h).

4.2. Zircon trace elements, and U–Th–Pb and Lu–Hf isotope analyses

Zircon grains were separated from bulk samples using standard magnetic and heavy liquid techniques. Representative grains were handpicked under a binocular microscope, mounted in epoxy resin, and then polished to expose the grain interiors. Prior to analysis, in order to choose the optimum laser targeting sites the zircons were examined in transmitted and reflected light as well with cathodoluminescence (CL) imaging to reveal their external and internal structures. The CL images were obtained by using a JEOL JSM6510 scanning electron microscope at Beijing Zircon Dating Navigation Technology Ltd., Beijing, China.

The LA-MC-ICP-MS zircon U–Pb dating and trace element determinations were undertaken using a Finnigan Neptune MC-ICP-MS instrument

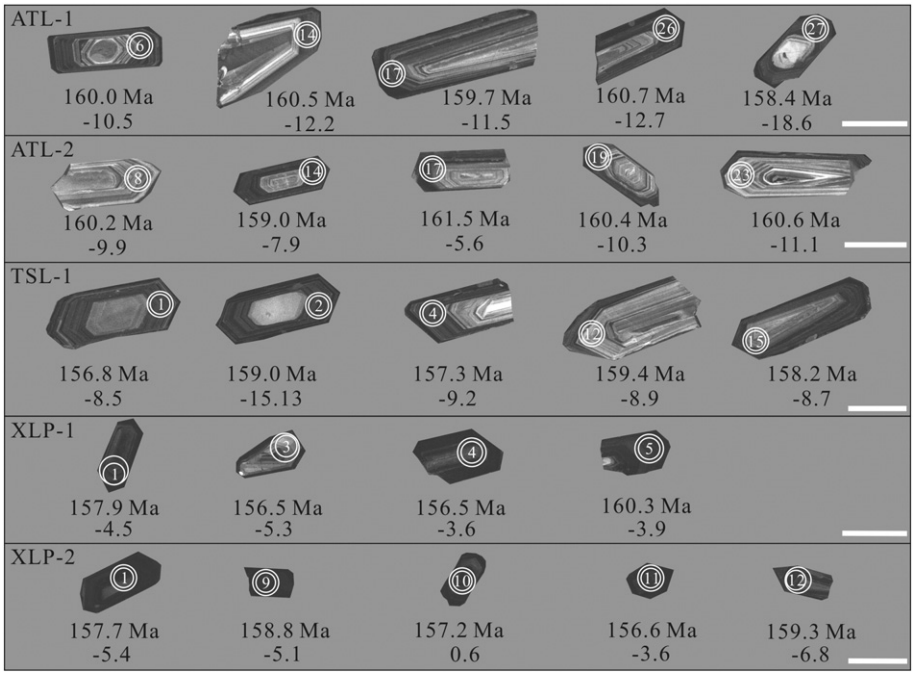

Fig. 7. Cathodoluminescence (CL) images of representative zircons separated from the Tongshanling granodiorite and the Xianglinpu granite. Small ellipses indicate the LA-MC-ICP-MS U–Pb analysis spots and the big circles indicate the LA-MC-ICP-MS analysis spots for Hf isotopes. Numbers near the analysis spots are the U–Pb ages and $\varepsilon_{Hf}(t)$ values. The white bars are 100 μm in length for scale. The U-Pb age date of the two Xianglinpu granite samples are from Zhao et al. (2016).

coupled to a New Wave UP 213 laser ablation system at the Key Laboratory of Metallogeny and Mineral Assessment, Institute of Mineral Resources, Beijing, China. Ablated material was transported towards the torch of the MC-ICP-MS instrument using He carrier gas, and analyses were undertaken using a 25 μm spot width and a 10 Hz repetition rate. Off-line selection and integration of the background and analytical signals, as well as time-drift correction and quantitative calibration for U–Pb dating, were undertaken using ICPMS Data Cal (Liu et al., 2008). The analytical approach taken was to conduct 5–10 measurements of unknown zircons between 3 measurements of the standard zircons GJ-1 (n = 2) and Plesovice (n = 1). Concordia diagrams and weighted mean calculations were made using Isoplot/Exversion 3.0 (Ludwig, 2003). The analytical procedures used during this study were similar to those described by Hou et al. (2009).

In situ Hf isotopic analyses of the zircons were carried out using a New Wave UP213 laser-ablation microprobe attached to a Neptune multi-collector ICP-MS at the Institute of Geology, Chinese Academy of Geological Sciences, Beijing, China. The instrumental conditions and the data acquisition methods have been described comprehensively by Hou et al. (2007). A stationary spot was used for analyses, with a beam diameter of ~44 μm depending on the size of ablated domains. Helium was used as a carrier gas to transport the ablated sample from the laser-ablation cell to the ICP-MS torch via a mixing chamber where it was mixed with argon. Zircon GJ1 was used as the reference standard, and the results for the standard are indistinguishable from the recommended weighted mean $^{176}Hf/^{177}Hf$ ratio of 0.282015 ± 19 (2σ) determined from *in situ* analyses by Elhlou et al. (2006). The measured $^{176}Hf/^{177}Hf$ ratios and the ^{176}Lu decay constant of 1.867×10^{-11} yr^{-1} reported by Söderlund et al. (2004) were used to calculate the initial $^{176}Hf/^{177}Hf$ ratios. The chondritic values of $^{176}Hf/^{177}Hf = 0.0336$ and $^{176}Lu/^{177}Hf = 0.282785$, reported by Bouvier et al. (2008), were used for the calculation of $\varepsilon_{Hf}(t)$ values. The depleted mantle line is defined by present-day $^{176}Hf/^{177}Hf = 0.28325$ and $^{176}Lu/^{177}Hf = 0.0384$ (Griffin et al., 2004). Because zircons are generally formed in granitic magmas that have been derived from felsic crust, the two-stage model ages (T_{2DM}) are more meaningful than the depleted mantle model ages.

4.3. Major and trace elements

Whole-rock major and trace element concentrations were determined at the Key Laboratory of Orogenic Belts and Crustal Evolution at the School of Earth and Space Sciences, Peking University, Beijing, China. The granite samples were first crushed to minus 200 mesh. For major element analyses, 50 mg samples of rock powder were fused with $LiBO_2$ in platinum crucibles at 980 °C, and the residues were subsequently dissolved in 10% HCl. For the trace element analyses, 100 mg samples of rock powder were accurately weighed in Savillex Teflon beakers, and a 5:3 mixture of HF:HNO_3 (and $HClO_4$) was added. The samples were digested at 110 °C, and the solutions subsequently diluted with 1% HNO_3 to a final volume of 100 ml. Major and trace elements were analyzed using a TJA ICAP9000 inductively coupled plasma–atomic emission spectrometer (ICP-AES). On the basis of analyses of international reference materials and replicate samples, the major and minor element oxides were estimated to be accurate to within 0.1% and 0.01%, respectively. The precision and accuracy of the trace element analyses were estimated to be better than 5%, except for Co, Ni, Nb, and Ta (better than 9%). The detailed analytical procedures followed those described by Liu et al. (2004, 2005).

4.4. Molybdenite Re–Os dating

The samples were crushed, separated, sieved, and handpicked under a binocular microscope to obtain monomineralic molybdenite with a purity >99%. The selected molybdenite grains were crushed in an agate mortar to about 200 mesh. The molybdenite analyzed during this study is fine grained (<0.1 mm), and thus the possible decoupling of Re and Os that occurs within large molybdenite grains is negligible (Stein et al., 2003; Selby and Creaser, 2004). The molybdenite Re–Os analyses were performed using a Thermo Electron TJA X-series ICP-MS instrument in the Re–Os Laboratory of the National Research Center of Geoanalysis, Chinese Academy of Geological Sciences, Beijing, China. The analytical procedures used during this study were similar to those

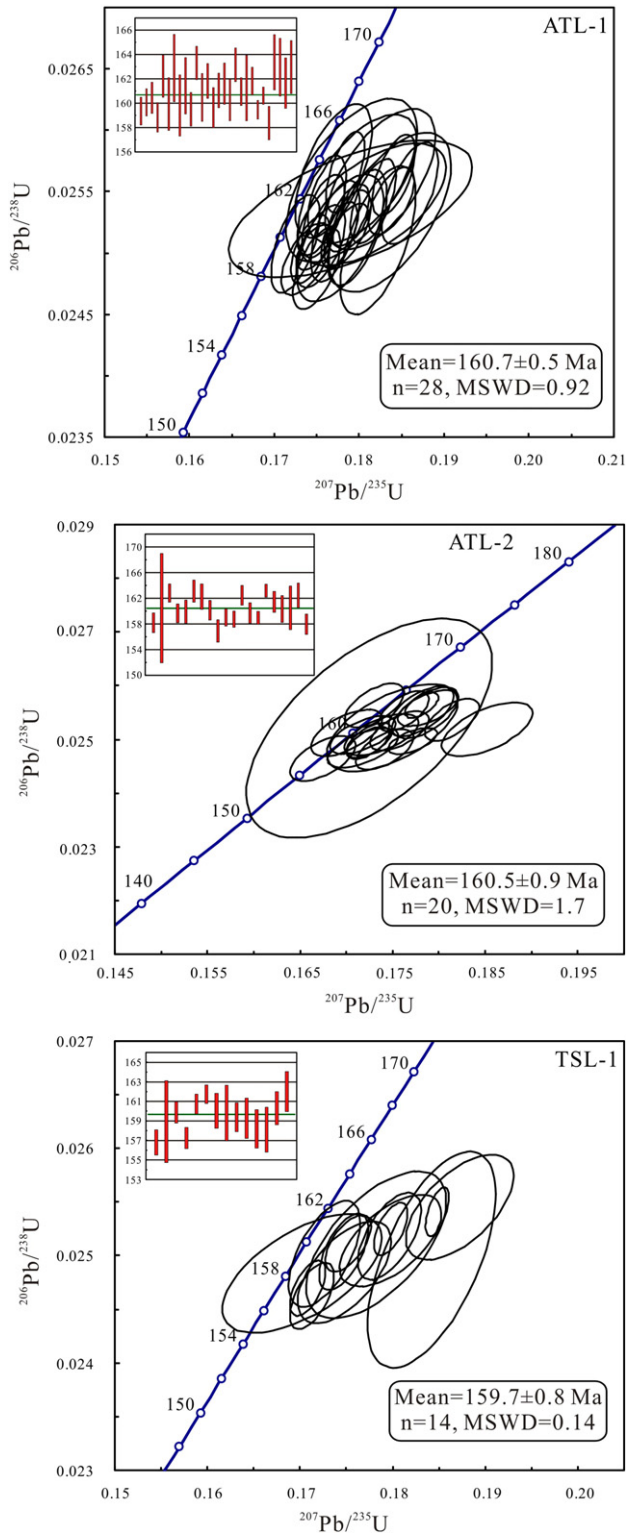

Fig. 8. LA-MC-ICP-MS zircon U–Pb concordia diagrams for the Tongshanling granodiorite porphyry in the Tongshanling orefield.

described by Du et al. (2009), Mao et al. (1999b), and Yuan et al. (2012b). The Re–Os model ages were calculated using $t = [\ln(1 + {}^{187}Os/{}^{187}Re)]/\lambda$, where λ is the decay constant of ^{187}Re at 1.666×10^{-11}/year (Smoliar et al., 1996). The Re–Os isochron age was calculated using the ISOPLOT 2.49 program (Ludwig, 2001).

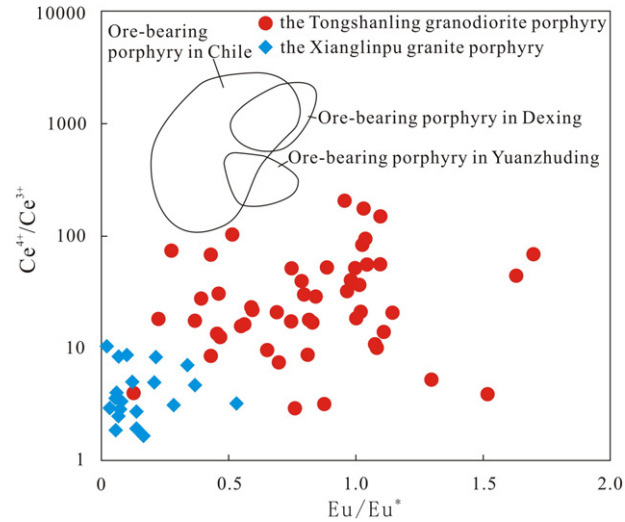

Fig. 9. Ce^{4+}/Ce^{3+} ratios *vs* Eu/Eu^* of zircon for the studied granitic rocks. Also shown are the data for the ore-bearing porphyry in Chile (Ballard et al., 2002), Dexing (Zhang et al., 2013a), and Yuanzhuding (Zhong et al., 2013).

5. Results

5.1. Zircon LA-MC-ICP-MS U–Pb geochronology

Zircon grains from the samples of Tongshanling granodiorite porphyry (ATL-1, ATL-2, and TSL-1) are euhedral and prismatic with aspect ratios of 1:1–3:1 and lengths of 100–300 μm. The grains are transparent and colorless under the optical microscope, and display concentric oscillatory zoning (Fig. 7). A small population of the grains possesses inherited cores, and all the analyses were made on the rims of the zircons. The age of each sample is given as the error-weighted mean of the common Pb-corrected $^{206}P/^{238}U$ age of the selected grains at the 95% confidence level. The *in situ* zircon LA-MC-ICP-MS U–Pb isotopic data are presented in Table 1 and illustrated on concordia plots in Fig. 8.

Zircons from samples ATL-1 and ATL-2 yielded U and Th concentrations of 84–1821 ppm and 39–723 ppm, respectively. Zircon Th/U ratios are between 0.18 and 1.08, indicating a magmatic origin (Hoskin and Black, 2000). Twenty-eight zircons from sample ATL-1 yielded a weighted mean age of 160.7 ± 0.5 Ma (MSWD = 0.92; Fig. 8) and 20 zircons from sample ATL-2 yielded a weighted mean age of 160.5 ± 0.9 Ma (MSWD = 1.7; Fig. 8), indicating that the crystallization age of the two samples is approximately 160 Ma.

Fourteen zircon grains were obtained from sample TSL-1, and their U and Th concentrations vary from 150 to 2314 ppm and 90 to 386 ppm, respectively; the Th/U ratios vary from 0.17 to 0.75. These zircons yielded a weighted mean age of 159.7 ± 0.8 Ma (MSWD = 0.14; Fig. 8), which is the best estimate for the crystallization age of sample TSL-1.

5.2. Trace elements and Ce^{4+}/Ce^{3+} values of the zircons

The results of the zircon trace-element analyses are presented in Supplementary Table 1. The values of the Ce^{4+}/Ce^{3+} ratios of the zircons were calculated using the method of Ballard et al. (2002), and the results are presented in Supplementary Table 1 and Fig. 9. Zircons from the Tongshanling granodiorite porphyry intrusion have Ce^{4+}/Ce^{3+} ratios in the range 2.8–207 (average of 37.1), clearly higher than the values of zircons from the Xianglinpu granite porphyry intrusion (0.9 to 10.1, average of 4.4). In addition, zircons from the Tongshanling granodiorite have Eu/Eu^* values of 0.13–1.70 (average of 0.8), notably higher than those of zircons from the Xianglinpu granite porphyry (0.02 to 0.55, average of 0.18) (Fig. 9).

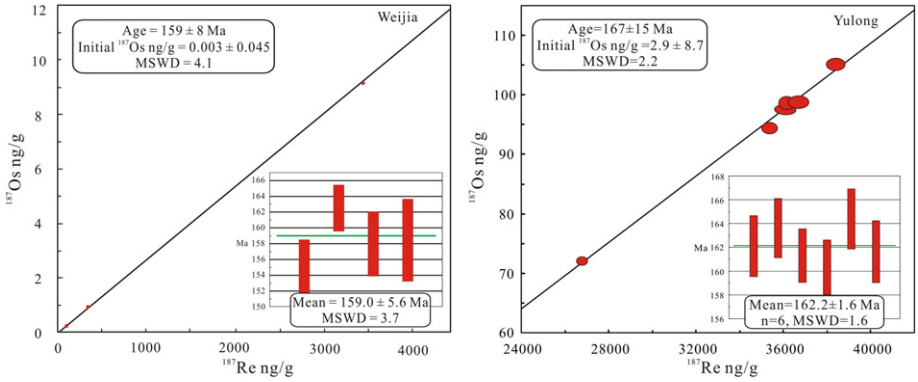

Fig. 10. Re–Os isochron age and weighted mean age for molybdenite separated from the Tongshanling Cu polymetallic deposit and Weijia W deposit.

5.3. Molybdenite Re–Os dating

The Re and Os contents of the molybdenite samples from the Tongshanling and Weijia deposits are listed in Table 2 and plotted on Fig. 10. The samples from the Tongshanling deposit have ^{187}Re and ^{187}Os contents of 26.7–38.3 ppm and 71.9–105.3 ppb, respectively, and they define relatively restricted model ages of 161.3 to 164.4 Ma, with a weighted mean age of 162.2 ± 1.6 Ma (MSWD = 1.6; Fig. 10). Although the Re–Os isochron age of 167 ± 15 Ma (MSWD = 2.2) has a fairly large error because there is little variation in the Re content of the molybdenite samples, the weighted average Re–Os model age of 162.2 ± 1.6 Ma represents the absolute age of the Mo deposit in the Yulong mine.

The molybdenite samples from the Weijia deposit have ^{187}Re and ^{187}Os contents of 0.1–3.5 ppm and 0.3–9.2 ppb, respectively. Four analyzed samples yielded a relatively narrow range of model ages (155.0–162.5 Ma), with a weighted mean age of 159.0 ± 5.6 Ma (MSWD = 3.7; Fig. 10). An isochron age of 159 ± 8 Ma (MWSD = 4.1) was calculated from the four samples. A zero intercept reveals that the molybdenite samples contain no detectable common ^{187}Os, which indicates that the model ages are reliable (Luck and Allègre, 1982; Selby and Creaser, 2004). The isochron age coincides well with the weighted average within error, also indicating that the molybdenite Re–Os dating is reliable.

5.4. Bulk-rock geochemistry

The results of geochemical analyses of samples from the Tongshanling granodiorite and Xianglinpu granite are listed in Table 3.The loss on ignition (LOI) for all samples was <2 wt%, indicating little post-magmatic alteration or weathering. The Xianglinpu granite porphyry is characterized by high contents of SiO_2 (72.55–74.30 wt%), and low MgO (0.17–0.35 wt%), total Fe_2O_3 (0.88–1.01 wt%), and CaO (0.80–0.89 wt%). Alkali contents are high, and Na_2O (3.26–3.99 wt%) is always less than K_2O (4.27–4.78 wt%). The A/CNK values [molar Al_2O_3/(CaO + Na_2O + K_2O)] are in the range 1.12–1.24, which is characteristic of

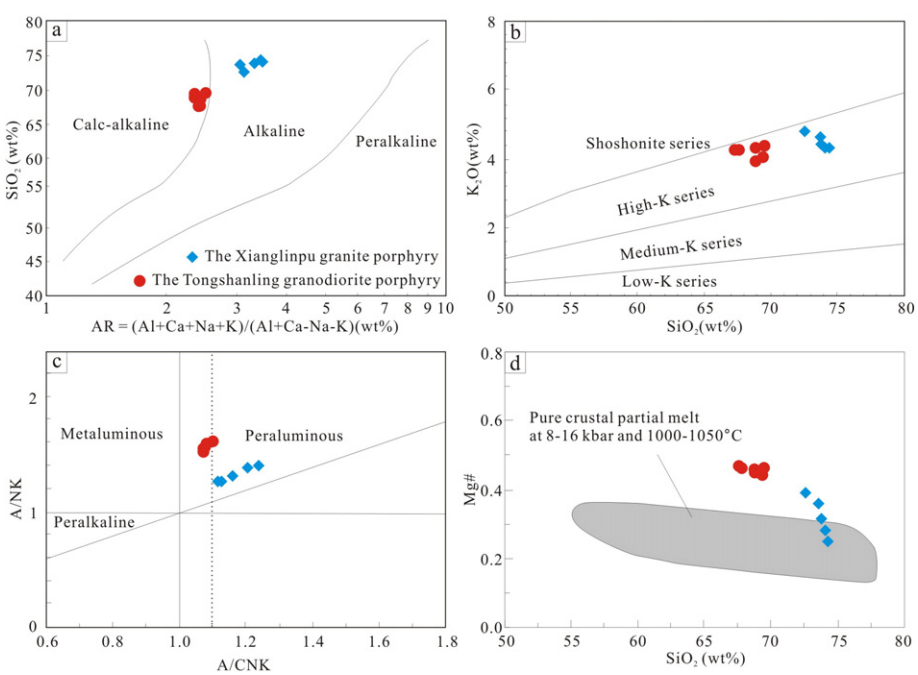

Fig. 11. SiO_2 *vs* alkalinity ratio (AR), K_2O vs SiO_2, A/NK vs A/CNK, and Mg# vs SiO_2 diagrams for the Tongshanling granodiorite and Xianglinpu granite porphyry (the compositional fields are from Maniar and Piccoli (1989), Middlemost (1994), Rollinson (1993), Rapp and Watson (1995), respectively; symbols of the studied porphyry intrusions in the following figures are the same as those in this figure).

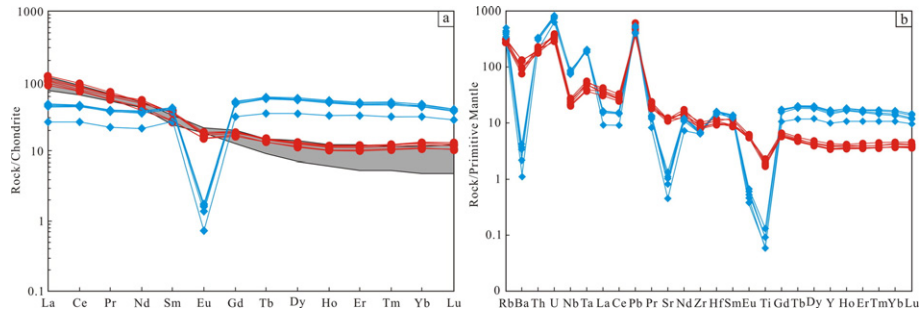

Fig. 12. Chondrite-normalized REE patterns and primitive mantle-normalized elements diagrams for the Tongshanling granodiorite and Xianglinpu granite porphyry. Also shown are the data of diorites associated with porphyry Cu deposits in the Escondida area, northern Chile (Richards et al., 2001). Normalization values are from Sun and McDonough (1989).

peraluminous granites (Fig. 11c). However, when compared with the Xianglinpu granite, the Tongshanling granodiorite has much lower SiO_2 contents (67.59–69.50 wt%), and higher MgO (1.26–1.67 wt%), total Fe_2O_3 (3.06–3.79 wt%), and CaO (2.24–2.43 wt%). The granodiorite is slightly peraluminous, with A/CNK values of 1.07–1.09. The Tongshanling granodiorite plots in the calc-alkali field, whereas the Xianglinpu granite plots in the alkaline field in the SiO_2 *vs* AR [AR = (Al + Ca + K + Na)/(Al + Ca–K–Na)] diagram (Fig. 11a). All the granitic rocks plot in the high-K field in the K_2O *vs* SiO_2 diagram (Fig. 11b).

The chondrite-normalized REE patterns of the two granites are clearly different to each other (Fig. 12a). The Xianglinpu granite is characterized by strong negative Eu anomalies ($Eu/Eu^* = 0.03–0.05$) and a slight enrichment in HREEs, with $(La/Yb)_N = 0.93–1.10$. In contrast, the Tongshanling granodiorite shows distinct LREE/HREE fractionation with $(La/Yb)_N = 7.97–10.19$ and relatively weak negative Eu anomalies ($Eu/Eu^* = 0.64–0.82$; Fig. 12a). In primitive-mantle-normalized variation diagrams (Fig. 12b), all the granite samples show enrichment in large ion lithophile elements (LILEs) relative to high field strength elements (HFSEs). However, the Xianglinpu granite is characterized by a much stronger enrichment in U and La, and a depletion in Ba, Nb, Ta, Sr, Eu, and Ti (Fig. 12b).

5.5. Zircon Hf isotopic compositions

The analyses of zircon Lu–Hf isotopes were undertaken in zircon grains which were analyzed for U–Pb geochronology. A total of 51 sets of $^{176}Hf/^{177}Hf$ isotopic data for zircons from five samples are listed in Supplementary Table 2 and plotted on Fig. 13.

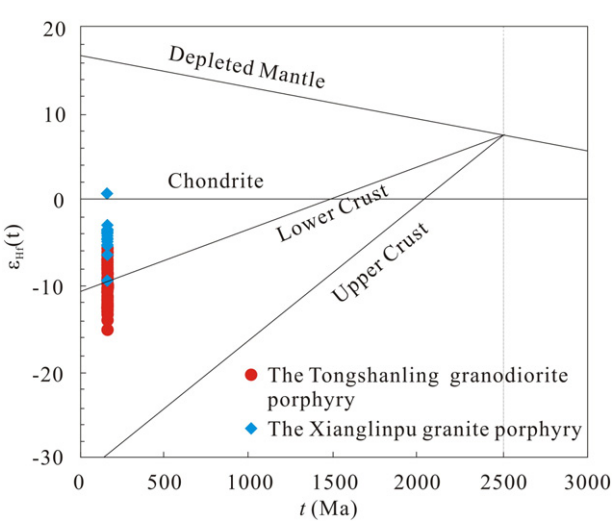

Fig. 13. Zircon Lu–Hf isotopic compositions of the studied granitic rocks.

Thirty-seven spot analyses were performed on zircons from the Tongshanling granodiorite. Zircon TSL-1-02 gave the lowest $\varepsilon_{Hf}(t)$ value of −15.1 and the oldest T_{DM2} of 2167 Ma. These values deviate significantly from those of the remaining zircons, which have $\varepsilon_{Hf}(t)$ values ranging between −13.9 and −5.6 (average −10.4), and T_{DM2} ages of 1567 to 2092 Ma (Fig. 14). These results display a multi-peak distribution of $\varepsilon_{Hf}(t)$ and T_{DM2} model ages, indicating that a late Paleoproterozoic crust was probably the major source material for the magma, together with some mantle-derived components.

Fourteen analytical results were obtained for zircons from two granite porphyry samples of the Xianglinpu granite. Zircon XLP-2-10 gave the highest $\varepsilon_{Hf}(t)$ of 0.6 and the youngest T_{DM2} of 1168 Ma. The remaining zircons have $\varepsilon_{Hf}(t)$ values that fall between −9.5 and −2.9, and the T_{DM2} model ages vary from 1394 to 1814 Ma (Fig. 14).

6. Discussion

6.1. Geochronology of the Tongshanling Cu and Weijia W deposits, and implications for regional mineralization

Several previous studies have examined the timing of emplacement of the granodiorite intrusion associated with the Tongshanling ore deposit (Wang et al., 2001; Wei et al., 2007; Jiang et al., 2009; Quan et al., 2013), yielding a wide range of ages (181–149 Ma). However, the age of the granodiorite responsible for the Cu mineralization remains unclear, because in most of the previous studies the localities of the samples were not specified. For our work, all the samples were collected from underground tunnels in the Tongshanling and Antangling mines (Fig. 3), and our results would therefore represent the age of the ore-forming granitic rock. LA-MC-ICP-MS U–Pb analysis of zircons from three granodiorite porphyry samples (ATL-1, ATL-2, and TSL-1) yielded weighted mean $^{206}Pb/^{238}U$ ages of 160.7 ± 0.5 Ma, 160.5 ± 0.9 Ma, and 159.7 ± 0.8 Ma, respectively, which are the same within error. Moreover, these data are consistent with newly reported SHRIMP zircon U–Pb dates (163.6 ± 2.1 Ma; Jiang et al., 2009), suggesting that the crystallization age of the ore-related granodiorite porphyry in this area can be constrained to ca.160 Ma.

The molybdenite samples collected from the Yulong mine in the Tongshanling deposit yield relatively restricted model ages of 161.3 to 164.4 Ma, with a weighted average age of 162.2 ± 1.6 Ma (MSWD = 1.6; Fig. 10). Therefore, the age of the Cu–(Mo)–Pb–Zn mineralization in the Tongshanling deposit can be constrained as ca.162 Ma, which is consistent with the emplacement age of the granodiorite porphyry. Integrating the zircon LA-MC-ICP-MS U–Pb

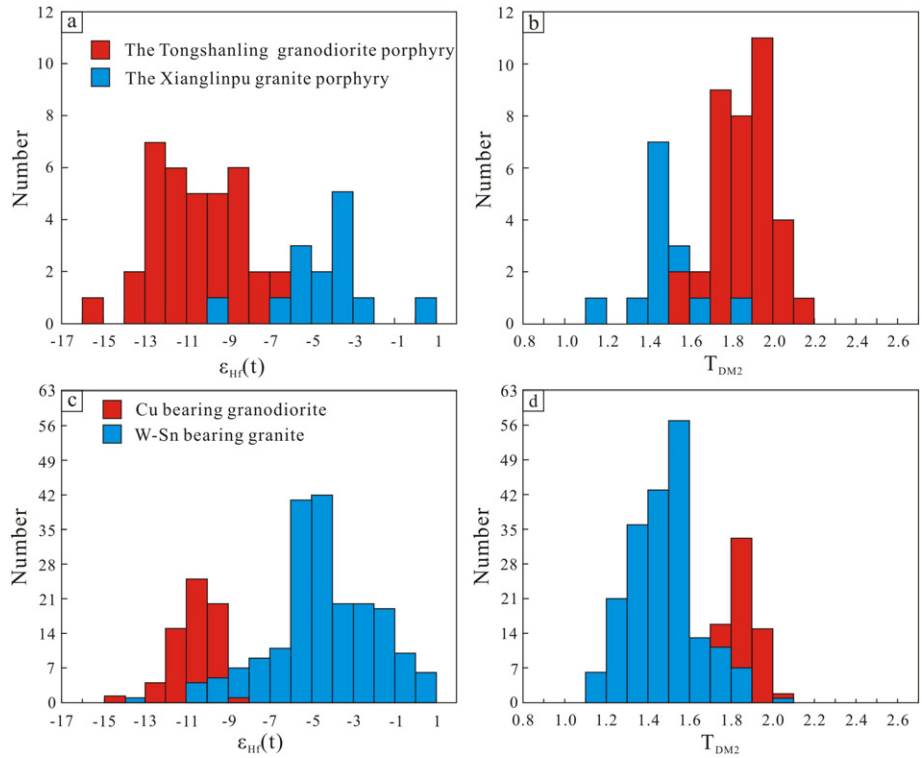

Fig. 14. Histogram of $\varepsilon_{Hf}(t)$ and T_{DM2} for the granitic rocks in the Tongshanling district (a, b) and the western part of the Nanling W–Sn province (c, d). (Hf isotopic composition data of zircon for the granites in the western part of the Nanling district are from Zhao et al., 2009, 2012; Liu et al., 2010; Huang et al., 2011; Zhu et al., 2011; Zuo et al., 2014).

and molybdenite Re–Os ages, we conclude that the Tongshanling Cu–(Mo)–Pb–Zn deposit was temporally, spatially, and genetically associated with the Tongshanling granodiorite porphyry, and that both were formed at ca.162–160 Ma.

The molybdenite samples from the Weijia W deposit yield consistent Re–Os isochron and model ages within error, and therefore the timing of W mineralization in the Weijia W deposit is estimated to be ca. 159 Ma, which is consistent with the zircon LA-MC-ICP-MS U–Pb age for the Xianglinpu granite porphyry (158 Ma; Zhao et al., 2016). Integrating these geochronologic data with the fact that the magmatic–hydrothermal alteration formed halos around the granite porphyry, we conclude that the Weijia W deposit is genetically related to the Xianglinpu granite, and that both formed at ca. 159–158 Ma.

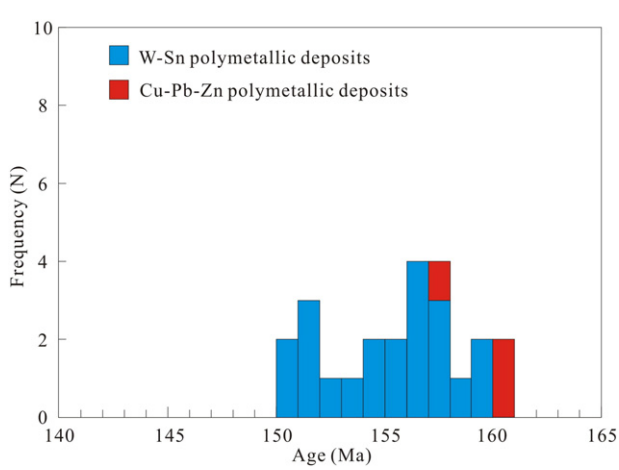

Fig. 15. Age histogram of W–Sn and Cu polymetallic deposits in southern Hunan (geochronological data for the W–Sn deposits are mainly based on Peng et al., 2008 and Mao et al., 2013).

Several previous attempts have been made to determine the timing differences of two contrasting ore deposits and their associated granitic rocks. It has been proposed that the Cu–Pb–Zn mineralization formed much earlier than the W–Sn mineralization in the Nanling Range (Hua et al., 2005; Mao et al., 2004, 2008). However, our results show that there is no significant time interval between the formation of the Cu–(Mo)–Pb–Zn mineralization and the W mineralization in the Tongshanling district, and that they both formed at ca.160 Ma. Moreover, recently reported precise geochronologic data show that the Baoshan Cu–Pb–Zn deposit and its associated granodiorite were formed at ca. 162–158 Ma (Lu et al., 2006; Xie et al., 2013), that the Shuikoushan Pb–Zn–Cu deposit and its associated granodiorite formed at ca.158 Ma (Huang et al., 2015), and that the Huangshaping Pb–Zn–Cu–W–Mo deposit and its associated granite porphyry formed at ca. 160–154 Ma (Yao et al., 2007; Yuan et al., 2014). Therefore, integrating those data with our new geochronologic data for the Tongshanling district, we conclude that the Cu–Pb–Zn mineralization in southern Hunan took place during the period of 162–154 Ma, at a similar time to, or slightly earlier than, the large-scale W–Sn mineralization in southern Hunan Province (160–150 Ma; Mao et al., 2013) (Fig. 15).

6.2. Sources of granitic magma in the Tongshanling district

Previous studies have shown that the hafnium isotopic compositions of zircon can constrain the nature of the magma source and the degree of magma mixing during the generation of granitic rocks (Griffin et al., 2002; Wang et al., 2003b; Hawkesworth and Kemp, 2006; Yang et al., 2007).

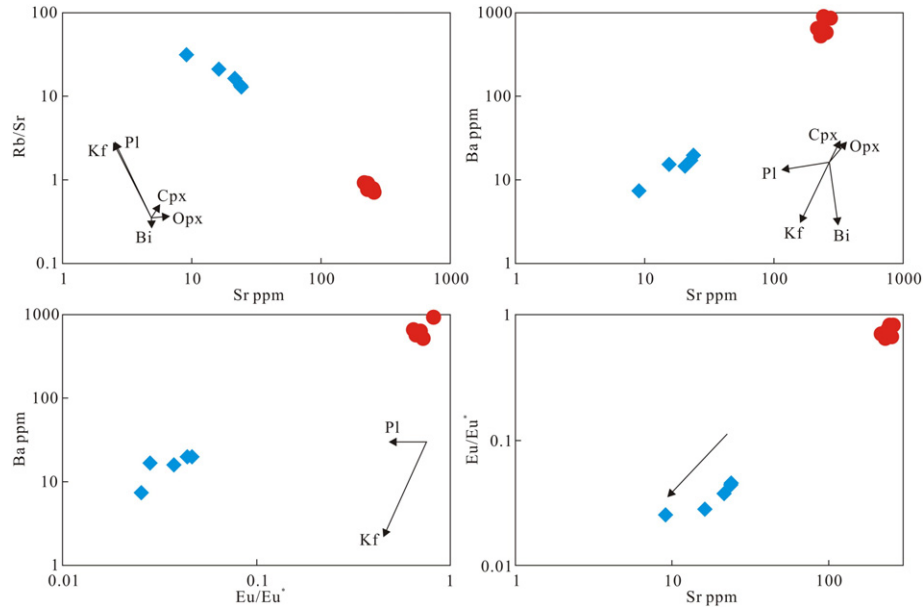

Fig. 16. Characteristics of the Tongshanling granodiorite and the Xianglinpu granite resulting from fractional crystallization. (Kf: K-feldspar. Pl: plagioclase. Bi: biotite. Cpx: clinopyroxene. Opx: orthopyroxene).

The Hf isotopic data for the magmatic zircons from the Tongshanling granodiorite and Xianglinpu granite exhibit variable negative $\varepsilon_{Hf}(t)$ values (−15.1 to −5.6 and −9.6 to 0.6, respectively) and provide T_{DM2} ages of 2.2–1.6 and 1.8–1.2 Ga, respectively. Such initial zircon Hf isotopic compositions indicate that the two granitic plutons were derived from the partial melting of Paleoproterozoic and Mesoproterozoic crustal materials respectively, possibly with minor contributions from the mantle (Li et al., 2007a). This interpretation is also supported by the presence of microgranular enclaves in both plutons (Fig. 6) and contemporaneous basaltic magmatism in the area (Jiang et al., 2009). In addition, both the Tongshanling granodiorite and Xianglinpu granite have higher values of Mg# than pure crustal partial melts (Fig. 11d), suggesting that some mantle-derived material was mixed with the crustal melts.

Although both the Tongshanling granodiorite and Xianglinpu granite were formed by the interaction of crust and mantle, different magma sources are indicated by the lower SiO_2 contents and $\varepsilon_{Hf}(t)$ values of the Tongshanling granodiorite. The listric-shaped REE patterns and the absence of obvious negative Eu anomalies for the Tongshanling granodiorite may be due to fractionation of middle + heavy REE-enriched hornblende and the suppression of feldspar fractionation (Richards et al., 2001; Wang et al., 2014), and such conditions arise where magmas contain sufficient water to stabilize hornblende as an early liquidus phase and suppress plagioclase crystallization (Richards et al., 2001; Annen et al., 2006). Thus, the Tongshanling granodiorite may have crystallized from a relatively hydrous magma. Furthermore, the bulk-rock Zr composition model of Watson and Harrison (1983) was used to calculate the zirconium-saturation temperatures (T_{zr}) for the Tongshanling granodiorite, and we obtained temperatures of 737–758 °C (Table 3). The presence of inherited zircons (Jiang et al., 2009) suggests that the temperatures could be maximum estimates of the initial magma temperatures at the source (Miller et al., 2003). Previous studies indicated that partial melting of the crust under low temperatures (≤800 °C) requires a hydrous magma source (Clemens and Watkins, 2001). This also suggests high water content in the source for the Tongshanling granodiorite. Although the water necessary for generating magma can be supplied by the breakdown of biotite, muscovite, or Ca-amphibole (Clemens and Watkins, 2001), only muscovite may undergo substantial dehydration at T < 800 °C (Miller et al., 2003). However, the Tongshanling granodiorite is weakly peraluminous with Al_2O_3 < 15 wt%, and thus its source may not have sufficient muscovite to supply the water necessary for generating magma (Xie et al., 2013). The granodiorite shows arc-like trace element signatures such as its negative anomalies of HFSEs (Nb, Ta, and Ti) and positive anomalies of LILEs (Rb, U, and Pb) in the primitive-mantle-normalized spider diagram (Fig. 12; Richards et al., 2001).These observations indicate that the southern Hunan area was quite similar to continental arc setting related to the subduction of the Paleo-Pacific Plate during the Jurassic (Li et al., 2007a; Mao et al., 2008, 2011b, 2013; Jiang et al., 2009). Thus, the water in the magma may have come from the mafic magmas that were derived from the partial melting of metasomatized and water-enriched lithospheric mantle, which is probably the main source of the Cu in the Tongshanling ore deposit. We conclude, therefore, that the Tongshanling granodiorite porphyry was formed by partial melting of crustal material induced by the injection of hydrous mafic magmas that were in turn derived from a subduction-modified lithospheric mantle. Furthermore, compared with other polymetallic Cu deposits in the Qin–Hang metallogenic belt, the $\varepsilon_{Hf}(t)$ values for zircons in the Tongshanling granodiorite are much lower than those for the Cu ore-bearing porphyry in Dexing (+3.4 to +6.9; Hou et al., 2013) and Yuanzhuding (+1.7 to +6.2; Zhong et al., 2013). Therefore, the amount of mafic magma (derived from the mantle or juvenile crust) that was incorporated into the ore-bearing porphyries provided the main control on the scale of Cu mineralization in the Qin-Hang metallogenic belt. This conclusion is consistent with the findings of Wang et al. (2015) and Hou et al. (2015a, 2015b), who studied porphyry Cu deposits in the Gangdese Belt, Tibet.

On the other hand, it is difficult to constrain the contribution of mafic magma to the Xianglinpu granite, due to its highly fractionated nature (Li et al., 2007b; Wu et al., 2003). The Xianglingpu granite has similar geochemical and isotopic characteristics to the W- and Sn-bearing granites of South China (Fig. 14). Most previous workers

Table 1
LA-MC-ICP-MS zircon U–Pb data of the Tongshanling granodiorite porphyry samples in the Tongshanling Cu–(Mo)–Pb–Zn polymetallic deposit, southern Hunan Province.

Spot no.	Concentrations (ppm)			Th/U	Isotopic ratios						Ages (Ma)					
	Pb	Th	U		$^{207}Pb/^{206}Pb$	1σ	$^{207}Pb/^{235}U$	1σ	$^{206}Pb/^{238}U$	1σ	$^{207}Pb/^{206}Pb$	1σ	$^{207}Pb/^{235}U$	1σ	$^{206}Pb/^{238}U$	1σ
Antangling-1 (mean = 160.7 ± 0.5 Ma, MSWD = 0.92, n = 28)																
ATL-1-1	98	154	465	0.33	0.0505	0.0003	0.1742	0.0015	0.0250	0.0002	216.7	11.1	163.0	1.3	159.4	1.1
ATL-1-2	160	223	1067	0.21	0.0513	0.0003	0.1776	0.0014	0.0251	0.0002	253.8	45.4	166.0	1.2	160.1	1.1
ATL-1-3	53	82	280	0.29	0.0514	0.0004	0.1785	0.0018	0.0252	0.0002	257.5	16.7	166.8	1.6	160.5	1.3
ATL-1-4	47	94	240	0.39	0.0505	0.0005	0.1737	0.0019	0.0250	0.0002	220.4	20.4	162.6	1.7	158.9	1.2
ATL-1-5	244	333	1821	0.18	0.0529	0.0002	0.1859	0.0022	0.0255	0.0003	324.1	11.1	173.1	1.9	162.3	1.7
ATL-1-6	91	144	437	0.33	0.0513	0.0005	0.1777	0.0033	0.0251	0.0003	253.8	20.4	166.1	2.9	160.0	2.1
ATL-1-7	158	218	533	0.41	0.0507	0.0009	0.1790	0.0051	0.0256	0.0004	227.8	75.0	167.2	4.4	162.9	2.8
ATL-1-9	327	551	1035	0.53	0.0527	0.0005	0.1821	0.0029	0.0251	0.0004	322.3	22.2	169.9	2.5	159.9	2.5
ATL-1-11	28	64	279	0.23	0.0511	0.0022	0.1789	0.0095	0.0254	0.0004	242.7	100.0	167.1	8.2	161.5	2.3
ATL-1-12	64	138	484	0.28	0.0507	0.0003	0.1754	0.0019	0.0251	0.0002	227.8	14.8	164.1	1.7	159.5	1.4
ATL-1-13	94	269	997	0.27	0.0504	0.0002	0.1783	0.0015	0.0257	0.0002	216.7	13.9	166.6	1.3	163.3	1.4
ATL-1-14	64	132	279	0.47	0.0518	0.0004	0.1797	0.0023	0.0252	0.0003	276.0	19.4	167.8	2.0	160.5	2.0
ATL-1-15	101	202	583	0.35	0.0518	0.0002	0.1816	0.0018	0.0254	0.0002	276.0	−23.1	169.4	1.5	161.9	1.4
ATL-1-17	115	283	919	0.31	0.0499	0.0002	0.1724	0.0019	0.0251	0.0003	190.8	4.6	161.5	1.6	159.7	1.7
ATL-1-18	112	233	853	0.27	0.0504	0.0002	0.1757	0.0016	0.0253	0.0002	213.0	4.6	164.4	1.4	161.1	1.4
ATL-1-19	154	343	858	0.40	0.0502	0.0002	0.1755	0.0019	0.0254	0.0003	211.2	9.3	164.2	1.6	161.6	1.7
ATL-1-20	183	445	843	0.53	0.0510	0.0003	0.1771	0.0019	0.0252	0.0003	242.7	14.8	165.6	1.6	160.3	1.7
ATL-1-21	66	118	305	0.39	0.0521	0.0003	0.1840	0.0017	0.0256	0.0002	300.1	13.0	171.5	1.4	163.2	1.4
ATL-1-22	61	162	150	1.08	0.0513	0.0004	0.1786	0.0016	0.0253	0.0002	253.8	18.5	166.9	1.4	161.0	1.1
ATL-1-23	54	107	212	0.50	0.0526	0.0011	0.1836	0.0047	0.0253	0.0004	309.3	50.9	171.1	4.1	161.3	2.7
ATL-1-24	79	169	424	0.40	0.0525	0.0004	0.1837	0.0018	0.0254	0.0002	305.6	10.2	171.2	1.5	161.9	1.1
ATL-1-25	80	153	445	0.34	0.0507	0.0004	0.1747	0.0014	0.0251	0.0001	233.4	16.7	163.5	1.2	159.5	0.8
ATL-1-26	87	229	329	0.70	0.0515	0.0003	0.1789	0.0014	0.0252	0.0001	264.9	13.0	167.1	1.2	160.7	0.7
ATL-1-27	127	302	676	0.45	0.0511	0.0003	0.1749	0.0018	0.0249	0.0002	255.6	13.0	163.7	1.6	158.4	1.4
ATL-1-28	139	237	874	0.27	0.0501	0.0006	0.1769	0.0030	0.0257	0.0004	211.2	27.8	165.4	2.6	163.4	2.3
ATL-1-29	20	39	84	0.46	0.0519	0.0009	0.1824	0.0043	0.0256	0.0004	279.7	40.7	170.2	3.7	163.0	2.4
ATL-1-32	25	62	85	0.73	0.0520	0.0014	0.1814	0.0058	0.0254	0.0003	283.4	61.1	169.3	5.0	161.7	2.1
ATL-1-33	36	63	135	0.47	0.0513	0.0009	0.1803	0.0042	0.0256	0.0003	257.5	38.9	168.3	3.6	163.0	2.2
Antangling-2 (mean = 160.5 ± 0.9 Ma, MSWD = 1.7, n = 20)																
ATL-2-1	127	311	605	0.51	0.0504	0.0004	0.1718	0.0025	0.0249	0.0002	213.0	18.5	160.9	2.2	158.3	1.5
ATL-2-2	64	131	244	0.54	0.0498	0.0003	0.1724	0.0088	0.0252	0.0013	187.1	13.0	161.5	7.6	160.5	8.5
ATL-2-3	153	323	903	0.36	0.0509	0.0003	0.1788	0.0022	0.0256	0.0002	235.3	16.7	167.0	1.9	162.9	1.4
ATL-2-4	69	175	385	0.45	0.0498	0.0004	0.1717	0.0023	0.0251	0.0002	187.1	21.3	160.9	2.0	159.8	1.5
ATL-2-5	64	132	251	0.52	0.0492	0.0005	0.1700	0.0025	0.0251	0.0003	166.8	−5.6	159.4	2.2	160.0	1.8
ATL-2-6	322	723	1418	0.51	0.0491	0.0002	0.1730	0.0021	0.0256	0.0003	153.8	11.1	162.0	1.8	163.2	1.7
ATL-2-7	89	184	382	0.48	0.0510	0.0004	0.1785	0.0024	0.0255	0.0003	242.7	12.0	166.7	2.0	162.3	2.0
ATL-2-8	97	196	314	0.62	0.0508	0.0004	0.1757	0.0021	0.0252	0.0002	231.6	21.3	164.3	1.8	160.2	1.5
ATL-2-9	84	197	316	0.62	0.0493	0.0004	0.1674	0.0023	0.0247	0.0003	164.9	23.1	157.2	2.0	157.0	1.7
ATL-2-10	86	171	723	0.24	0.0501	0.0002	0.1724	0.0016	0.0250	0.0002	211.2	9.3	161.5	1.4	159.1	1.3
ATL-2-11	156	329	694	0.47	0.0502	0.0002	0.1723	0.0015	0.0249	0.0002	211.2	11.1	161.4	1.3	158.8	1.2
ATL-2-12	137	261	743	0.35	0.0501	0.0002	0.1761	0.0018	0.0255	0.0002	198.2	11.1	164.7	1.5	162.6	1.5
ATL-2-13	268	534	1752	0.30	0.0502	0.0004	0.1737	0.0027	0.0251	0.0003	211.2	25.0	162.7	2.3	159.8	1.6
ATL-2-14	102	170	216	0.79	0.0514	0.0004	0.1771	0.0017	0.0250	0.0002	261.2	18.5	165.6	1.5	159.0	1.0
ATL-2-15	187	307	1079	0.28	0.0504	0.0002	0.1781	0.0012	0.0256	0.0002	213.0	4.6	166.4	1.0	163.3	1.0
ATL-2-17	241	355	934	0.38	0.0519	0.0003	0.1814	0.0019	0.0254	0.0003	279.7	−16.7	169.2	1.7	161.5	1.6
ATL-2-19	90	87	418	0.21	0.0533	0.0007	0.1852	0.0032	0.0252	0.0003	342.7	23.1	172.5	2.8	160.4	2.1
ATL-2-23	95	125	272	0.46	0.0503	0.0009	0.1749	0.0047	0.0252	0.0005	209.3	43.5	163.7	4.0	160.6	3.4
ATL-2-24	143	200	810	0.25	0.0506	0.0003	0.1780	0.0023	0.0255	0.0003	220.4	11.1	166.3	2.0	162.5	1.9
ATL-2-25	67	108	251	0.43	0.0509	0.0005	0.1741	0.0021	0.0248	0.0002	235.3	20.4	163.0	1.8	158.0	1.6
Tongshanling-1 (mean = 159.7 ± 0.8 Ma, MSWD = 0.14, n = 14)																
TSL-1-1	131	175	948	0.18	0.0504	0.0003	0.1712	0.0016	0.0246	0.0002	216.7	8.3	160.5	1.4	156.8	1.3
TSL-1-2	109	131	693	0.19	0.0536	0.0007	0.1842	0.0046	0.0250	0.0007	353.8	32.4	171.6	3.9	159.0	4.2
TSL-1-3	92	122	284	0.43	0.0506	0.0004	0.1751	0.0016	0.0251	0.0002	233.4	13.9	163.9	1.4	159.9	1.1
TSL-1-4	161	232	1026	0.23	0.0501	0.0002	0.1708	0.0013	0.0247	0.0002	211.2	11.1	160.1	1.1	157.3	1.1
TSL-1-5	206	246	1203	0.20	0.0517	0.0002	0.1797	0.0012	0.0253	0.0002	333.4	9.3	167.8	1.0	160.8	1.0
TSL-1-6	325	386	2314	0.17	0.0527	0.0004	0.1848	0.0008	0.0254	0.0002	316.7	23.1	172.2	0.7	161.8	0.9
TSL-1-10	66	112	150	0.75	0.0518	0.0008	0.1797	0.0036	0.0251	0.0003	276.0	41.7	167.8	3.1	160.1	1.8
TSL-1-11	49	111	210	0.53	0.0513	0.0008	0.1782	0.0050	0.0251	0.0005	253.8	41.7	166.5	4.3	159.8	2.8
TSL-1-12	97	209	807	0.26	0.0506	0.0002	0.1747	0.0017	0.0250	0.0002	233.4	9.3	163.5	1.5	159.4	1.5
TSL-1-13	48	103	228	0.45	0.0500	0.0004	0.1726	0.0025	0.0250	0.0003	198.2	12.0	161.7	2.2	159.3	2.1
TSL-1-15	50	108	186	0.58	0.0509	0.0007	0.1747	0.0033	0.0249	0.0003	239.0	63.9	163.5	2.9	158.2	2.0
TSL-1-16	106	314	454	0.69	0.0498	0.0023	0.1702	0.0057	0.0248	0.0004	183.4	107.4	159.6	4.9	158.2	2.3
TSL-1-17	64	166	399	0.42	0.0517	0.0003	0.1796	0.0022	0.0252	0.0003	272.3	13.0	167.7	1.9	160.4	1.7

have favored a crustal melt source for these magmas, possibly with some input from asthenospheric mantle material during rollback of the Paleo-Pacific Plate or by subduction of a slab window (Mao et al., 2006; Jiang et al., 2009; Mao et al., 2014). Considering its relatively high $\varepsilon_{Hf}(t)$ values and young T_{DM} ages, we propose that the Xianglinpu granite was derived from the anatexis of old crustal material in response to the injection of magmas derived from the asthenospheric mantle.

Table 2
Molybdenite Re–Os values of the Weijia W deposit and Yulong Mo mine, southern Hunan Province.

Analyses no.	Sample no.	Weight (g)	Re (ppb)		Common Os (ppb)		^{187}Re (ppb)		^{187}Os (ppb)		Model ages (Ma)	
			Measured	2σ	Measured	2σ	Measured	2σ	Measured	2σ	Measured	2σ
Molybdenite Re–Os values of the Yulong mine												
120903-1	YL-1	0.02066	57,418.78	641.90	4.4003	0.0339	36,088.85	403.46	97.61	0.77	162.1	2.6
120903-2	YL-2	0.02055	57,524.42	481.74	6.4442	0.1212	36,155.25	302.79	98.71	0.97	163.7	2.5
120903-3	YL-3	0.02008	42,501.15	313.99	1.2993	0.0619	26,712.82	197.35	71.90	0.62	161.3	2.2
120903-4	YL-4	0.02015	56,226.15	471.89	1.2110	0.0723	35,339.26	296.60	94.53	0.79	160.4	2.3
120903-5	YL-5	0.02057	61,069.31	601.36	9.3622	0.1224	38,383.28	377.98	105.28	0.91	164.4	2.5
120903-6	YL-6	0.02063	58,345.62	619.20	1.9305	0.0499	36,671.39	389.19	98.89	0.89	161.7	2.6
Molybdenite Re–Os values of the Weijia W deposit												
150408-18	XLP-4	0.01154	151.10	1.20	0.1010	0.0020	95.00	0.73	0.25	0.00	155.0	3.5
150408-19	XLP-5	0.00786	549.90	4.60	0.1270	0.0010	345.60	2.90	0.94	0.10	162.5	3.0
150408-20	XLP-6	0.01096	5531.00	124.00	0.1070	0.0080	3476.00	78.00	9.16	0.08	158.0	4.1
150408-21	XLP-7	0.01099	158.70	1.20	0.1680	0.0080	99.75	0.74	0.26	0.01	158.5	5.1

6.3. Nature of the granitic rocks

6.3.1. Redox state of the ore-related granitic rocks

The relative oxidation state of magma is important in controlling the compatible or incompatible nature of many ore elements (Candela and Bouton, 1990; Blevin and Chappell, 1992, 1995; Sillitoe, 2010; Sun et al., 2013). Previous workers have suggested that granitic rocks related to Cu mineralization generally crystallize from oxidized magma, and that those associated with Sn deposits crystallize from relatively reduced magma. On the other hand, those related to W mineralization have little dependence on the redox state of the magma (Blevin and Chappell, 1992, 1995; Mungall, 2002). These relationships depend on the fact that the magmatic redox state plays an important role in the speciation and solubility of sulfur, and the valence state of ore-forming elements in silicate melts, which in turn influences the solubility and behavior of those ore elements (Štemprok, 1990; Wood and Samson, 2000; Linnen and Cuney, 2005; Che et al., 2013; Wang et al., 2014).

Zircon is a good recorder of oxygen fugacity and zircons crystallized from an oxidized magma generally have large Ce anomalies and high Ce^{4+}/Ce^{3+} values (Ballard et al., 2002; Hanchar and Van Westrenen, 2007; Qiu et al., 2013). Our study has shown that most zircons from the Tongshanling granodiorite have much higher Ce^{4+}/Ce^{3+} ratios (average 37.1) than those of the Xianglinpu granite porphyry (average 4.4). This indicates that the Cu–(Mo)–Pb–Zn ore-bearing granodiorite porphyry had a higher fO_2 than the W mineralized granite porphyry, which is consistent with the conclusions made on the basis of compositions of apatite from granitic rocks in southeastern Hunan Province (Ding et al., 2015). The relatively high fO_2 of the Tongshanling granodiorite may have been the result of the input of melts derived from a lithospheric mantle that had been modified by hydrous fluids generated from a subducting slab (Wang et al., 2014; Kelley and Cottrell, 2009) However, the Ce^{4+}/Ce^{3+} ratios of zircons from the Tongshanling granodiorite are much lower than those reported from the ore-bearing porphyry of the Dexing and Yuanzhuding giant porphyry copper deposits (Fig. 9). This may be an important constraint on why the Tongshanling is merely a middle-scale copper deposit.

6.3.2. Fractional crystallization

The significant depletions in Ba, Sr, Eu, and Ti shown in the spider diagrams (Fig. 12) indicate significant fractional crystallization during the formation of the Xianglinpu granite porphyry (Wu et al., 2003). Separation of Ti-bearing phases (ilmenite, titanite, etc.) would have resulted in depletions of Ti, Nb, and Ta. Strong Eu depletion is thought to be related to the fractionation of plagioclase and/or K-feldspar. This is also confirmed by the correlations between Sr and Rb/Sr, Ba, and Eu/Eu*, and the positive correlation between Eu/Eu* and Ba (Fig. 16). In addition, the high Rb/Sr and Sm/Nd ratios, and low Th/U and Ba/Rb ratios also indicate that the Xianglinpu granitic magma underwent intensive fractional crystallization (Table 3; Blevin and Chappell, 1992). Furthermore, the REE patterns of the Xianglinpu granite porphyries exhibit the M-type tetrad effect and a strong depletion in Eu (Fig. 12), similar to many W-Sn-bearing granitic plutons in the Nanling W–Sn province (Mao and Li, 1995; Zhao et al., 2002; Li et al., 2007b; Xuan et al., 2014). The REE tetrad effect is shared by a number of highly evolved granitic rocks (Masuda et al., 1987; McLennan, 1994; Irber, 1999; Monecke et al., 2002) and it is generally thought to be caused by fluid–melt interaction in highly evolved melts (Jahn et al., 2001; Zhao et al., 2002). Thus, this also indicates that the Xianglinpu granite porphyry underwent intensive fractional crystallization, which is favorable for tungsten mineralization (Blevin and Chappell, 1995). In contrast, there was no obvious fractional crystallization during the formation of the Tongshanling granodiorite porphyry (Fig. 16; Table 3).

7. Conclusions

New geological, petrologic, geochemical, and isotopic data on the Tongshanling granodiorite porphyry and the Xianglinpu granite porphyry in southern Hunan Province allow us to draw the following conclusions.

1) Molybdenite Re–Os ages (162 Ma) and zircon U–Pb ages (160 Ma) indicate that the emplacement of the Tongshanling granodiorite porphyry and the formation of the associated Cu–(Mo)–Pb–Zn mineralization took place at ca. 162–160 Ma, slightly earlier than the formation of the Weijia W deposit at ca. 159 Ma (molybdenite Re–Os ages). Combining our new data with earlier published information, we suggest that there is no obvious time gap between the Cu polymetallic mineralization and the major W–Sn mineralization in southern Hunan Province.
2) Geochemical and *in situ* zircon Hf isotopic data indicate that the Tongshanling granodiorite porphyry was formed by partial melting of Paleoproterozoic crustal material in response to the injection of hydrous mafic magma that in turn was derived from subduction-modified lithospheric mantle. On the other hand, the Xianglinpu granite porphyry might have been derived by anatexis of a Mesoproterozoic crustal source in response to the injection of magma derived from the asthenospheric mantle. These different processes explain the different types of mineralization in the Tongshanling district.
3) The average Ce^{4+}/Ce^{3+} values of zircons from the Tongshanling granodiorite porphyry (37.1) are much higher than those of zircons

Table 3
Major (wt%) and trace element (ppm) compositions of the Tongshanling granodiorite porphyry and the Xianglinpu granite porphyry in the Tongshanling district.

Sample	TSL-3-1	TSL-3-2	TSL-3-3	TSL-3-4	TSL-3-5	TSL-3-6	XLP-1	XLP-2	XLP-4	XLP-5	XLP-6
Rock type	Granodiorite porphyry						Granite porphyry				
SiO_2	68.83	69.42	67.59	69.50	68.84	67.66	73.62	74.30	72.55	74.13	73.82
Al_2O_3	15.05	14.75	14.94	14.50	14.75	14.95	14.74	14.17	14.99	14.18	14.35
$^{T}Fe_2O_3$	3.06	3.17	3.78	3.10	3.22	3.79	0.88	1.01	0.95	0.99	0.95
CaO	2.38	2.43	2.43	2.24	2.41	2.37	0.82	0.81	0.89	0.80	0.80
MgO	1.28	1.26	1.66	1.32	1.31	1.67	0.24	0.17	0.35	0.19	0.22
K_2O	4.30	4.02	4.24	4.36	3.92	4.21	4.65	4.30	4.78	4.27	4.43
Na_2O	2.85	2.93	2.96	2.87	3.03	3.03	3.26	3.95	3.43	3.99	3.72
MnO	0.07	0.06	0.07	0.06	0.06	0.07	0.02	0.03	0.02	0.03	0.03
TiO_2	0.35	0.35	0.47	0.36	0.36	0.48	0.02	0.01	0.03	0.02	0.02
P_2O_5	0.13	0.14	0.17	0.14	0.13	0.18	0.01	0.01	0.02	0.01	0.01
Total	99.73	99.68	99.59	99.72	99.67	99.59	99.91	99.91	99.89	99.91	99.93
LOI	1.44	1.15	1.27	1.26	1.63	1.17	1.64	1.14	1.90	1.29	1.57
FeO	1.90	2.24	2.82	2.23	2.35	2.83	0.55	0.67	0.55	0.67	0.55
Fe_2O_3	0.95	0.68	0.65	0.62	0.61	0.65	0.27	0.27	0.33	0.25	0.34
Mg#	0.46	0.44	0.47	0.46	0.45	0.47	0.36	0.25	0.42	0.28	0.31
Li	37.6	37.8	31.0	36.4	34.1	29.4	6.3	11.1	6.3	9.9	8.9
Be	3.24	3.82	3.66	2.96	3.43	3.48	10.6	9.75	10.7	9.85	10.7
Sc	6.60	7.07	11.4	6.58	6.47	7.62	8.84	9.07	9.20	6.87	9.43
Ti	2111	2307	2801	2113	2117	2712	144	76	142	76	119
V	38.7	42.2	52.0	38.6	38.5	49.6	0.91	0.98	0.85	0.82	1.06
Cr	33.7	37.2	37.3	35.8	37.8	31.9	45.5	54.9	38.8	42.8	53.8
Mn	465	472	487	456	431	466	173	200	171	198	195
CO	5.14	8.42	6.39	7.50	5.84	5.99	0.58	0.28	0.18	0.13	0.12
Ni	4.23	5.09	5.29	8.88	4.34	5.06	8.79	1.49	2.97	1.49	1.42
Cu	6.81	12.21	19.49	11.94	7.80	17.91	2.07	2.46	2.30	1.53	1.60
Zn	46.2	52.6	64.5	54.4	47.1	52.6	40.2	52.9	38.9	50.7	44.4
Ga	15.6	17.6	17.1	15.3	15.8	16.0	28.1	28.1	27.9	27.7	29.8
Rb	186	199	210	190	177	200	319	338	318	283	347
Sr	260	254	231	247	231	218	24.0	16.3	23.9	9.14	21.6
Y	15.4	17.3	19.4	15.6	15.4	17.8	65.7	73.8	64.1	46.1	73.0
Zr	88.0	101	114	93.5	92.4	107	77.3	75.3	74.0	73.1	74.2
Nb	14.4	16.5	18.7	14.0	15.1	17.7	54.4	52.8	53.9	53.8	56.6
Mo	2.07	2.22	1.93	2.28	1.83	1.72	4.43	3.27	3.25	2.81	3.61
Sn	2.09	2.27	2.46	2.10	2.07	2.33	3.08	11.5	3.18	11.7	7.32
Ca	8.33	10.0	10.9	7.96	9.05	10.3	10.9	13.8	10.9	13.5	12.7
Ba	929	571	660	917	519	635	18.6	16.6	19.7	7.3	15.8
La	24.9	29.2	25.8	21.6	25.1	23.3	10.1	10.5	10.7	6.18	11.0
Ce	47.9	56.6	51.8	42.0	49.0	45.9	24.9	25.2	25.9	15.7	26.7
Pr	5.30	6.28	5.72	4.74	5.44	5.10	3.36	3.46	3.52	2.09	3.62
Nd	19.1	23.5	21.2	17.0	20.5	17.6	15.9	16.6	16.6	9.96	17.2
Sm	4.08	5.37	5.03	3.90	4.09	4.01	5.50	6.17	6.00	4.00	6.00
Eu	1.02	1.00	0.95	0.98	0.90	0.88	0.11	0.07	0.11	0.04	0.10
Gd	3.57	3.99	4.06	3.45	3.54	3.71	9.69	10.4	9.76	6.39	10.5
Tb	0.51	0.56	0.60	0.50	0.50	0.54	2.01	2.13	2.03	1.30	2.16
Dy	2.94	3.22	3.53	2.93	2.90	3.19	13.5	14.3	13.6	8.80	14.4
Ho	0.58	0.63	0.69	0.58	0.56	0.66	2.81	2.90	2.76	1.80	2.98
Er	1.67	1.87	2.07	1.67	1.67	1.87	7.55	8.23	7.56	5.25	8.21
Tm	0.26	0.30	0.33	0.26	0.27	0.30	1.10	1.25	1.11	0.80	1.21
Yb	1.81	2.05	2.24	1.80	1.83	2.10	6.90	8.15	7.01	5.24	7.71
Lu	0.27	0.30	0.34	0.27	0.27	0.31	0.90	1.08	0.91	0.71	1.01
Hf	2.84	3.37	3.65	3.04	3.04	3.37	4.86	4.97	4.74	5.06	4.98
Ta	1.57	2.18	2.34	1.49	2.00	2.04	8.08	8.63	8.15	8.71	8.88
W	80.8	24.1	14.5	9.84	6.82	4.35	23.6	14.5	22.5	13.6	15.8
Pb	28.2	29.5	27.8	28.6	26.2	26.6	41.7	44.7	42.8	39.3	43.9
Th	16.6	19.4	16.4	15.5	17.3	15.0	26.5	27.4	26.4	16.3	27.8
U	6.12	7.52	8.12	8.00	7.53	6.61	16.5	17.7	16.3	13.5	17.7
Rb/Sr	0.72	0.78	0.91	0.77	0.76	0.92	13.32	20.79	13.31	30.98	16.07
Sm/Nd	0.21	0.23	0.24	0.23	0.20	0.23	0.35	0.37	0.36	0.40	0.35
Th/U	2.71	2.57	2.02	1.93	2.30	2.27	1.61	1.55	1.62	1.20	1.57
Ba/Rb	4.99	2.87	3.15	4.81	2.94	3.17	0.06	0.05	0.06	0.03	0.05
$(La/Yb)_N$	9.83	10.19	8.26	8.60	9.84	7.97	1.05	0.93	1.10	0.85	1.02
Eu/Eu^*	0.82	0.66	0.64	0.82	0.72	0.70	0.05	0.03	0.04	0.03	0.04
T_{zr} (°C)	737.4	748.7	758.0	742.2	741.3	752.8	742.8	740.7	739.3	738.4	739.5

from the Xianglinpu granite porphyry (5.5), which indicates that the Tongshanling granodiorite was derived from more oxidized magma. Furthermore, the Tongshanling granodiorite underwent less fractional crystallization than the Xianglinpu granite. These differences may provide important constraints on the different types of mineralization associated with these two intrusive bodies.

4) Compared with other Jurassic Cu deposits in the Qin–Hang metallogenic belt, the relatively small contribution of mantle-derived material and the relatively low fO_2 of the ore-forming

porphyry in the Tongshanling district may have been the main reasons why giant porphyry copper deposits did not form in this area.

Supplementary data to this article can be found online at http://dx.doi.org/10.1016/j.oregeorev.2016.03.004.

Acknowledgments

This work was jointly supported by the National Basic Research Program of China (No. 2012CB416704), the National Natural Science Foundation of China (Nos. 41173052, 41373047, 40903020), and the National Nonprofit Natural Science Foundation of China (K1204). The authors are grateful for Prof. Franco Pirajno, Dr. Yener EYUBOGLU and an anonymous reviewer for their valuable comments that greatly improved the manuscript.

References

Annen, C., Blundy, J., Sparks, R., 2006. The genesis of intermediate and silicic magmas in deep crustal hot zones. J. Petrol. 47, 505–539.
Ballard, J.R., Palin, M.J., Campbell, I.H., 2002. Relative oxidation states of magmas inferred from Ce(IV)/Ce(III) in zircon: application to porphyry copper deposits of northern Chile. Contrib. Mineral. Petrol. 144, 347–364.
Blevin, P.L., Chappell, B.W., 1992. The role of magma sources, oxidation states and fractionation in determining the granite metallogeny of eastern Australia: transactions of the Royal Society of Edinburgh. Earth Sci. 83, 305–316.
Blevin, P.L., Chappell, B.W., 1995. Chemistry, origin, and evolution of mineralized granites in the Lachlan fold belt, Australia; the metallogeny of I-and S-type granites. Econ. Geol. 90, 1604–1619.
Bouvier, A., Vervoort, J.D., Patchett, P.J., 2008. The Lu–Hf and Sm–Nd isotopic composition of CHUR: constraints from unequilibrated chondrites and implications for the bulk composition of terrestrial planets. Earth Planet. Sci. Lett. 273, 48–57.
Cai, Y.X., Tan, J.J., Yang, H.M., Lu, S.S., Duan, R.C., Qiu, X.F., Cheng, S.B., Yang, X.L., 2015. The origin of ore-forming material in the Tongshanling Cu-polymetallic ore field in Hunan Province: constrains from S–Pb–C isotopes. Acta Geol. Sin. 89, 1792–1803 (in Chinese with English abstract).
Candela, P.A., Bouton, S.L., 1990. The influence of oxygen fugacity on tungsten and molybdenum partitioning between silicate melts and ilmenite. Econ. Geol. 85, 633–640.
Che, X.D., Linnen, R.L., Wang, R.C., Aseri, A., Thibault, Y., 2013. Tungsten solubility in evolved granitic melts: an evaluation of magmatic wolframite. Geochim. Cosmochim. Acta 106, 84–98.
Chen, C.H., Lee, C.Y., Shinjo, R., 2008. Was there Jurassic paleo-Pacific subduction in South China?: constraints from 40 Ar/39 Ar dating, elemental and Sr–Nd–Pb isotopic geochemistry of the Mesozoic basalts. Lithos 106, 83–92.
Chen, J., Jahn, B.M., 1998. Crustal evolution of southeastern China: Nd and Sr isotopic evidence. Tectonophysics 284, 101–133.
Clemens, J., Watkins, J., 2001. The fluid regime of high-temperature metamorphism during granitoid magma genesis. Contrib. Mineral. Petrol. 140, 600–606.
Ding, T., Ma, D., Lu, J., Zhang, R., 2015. Apatite in granitoids related to polymetallic mineral deposits in southeastern Hunan Province, Shi–Hang zone, China: implications for petrogenesis and metallogenesis. Ore Geol. Rev. 69, 104–117.
Du, A.D., Qu, W.J., Li, C., Yang, G., 2009. A review on the development of Re–Os isotopic dating methods and techniques. Rock Miner. Anal. 28, 288–304 (in Chinese with English abstract).
Elhlou, S., Belousova, E., Griffin, W.L., Pearson, N.J., O'Reilly, S.Y., 2006. Trace element and isotopic composition of GJ-red zircon standard by laser ablation. Geochim. Cosmochim. Acta 70, A158.
Faure, M., Ishida, K., 1990. The Mid-Upper Jurassic olistostrome of the west Philippines: a distinctive key-marker for the North Palawan block. J. SE Asian Earth Sci. 4, 61–67.
Griffin, W., Wang, X., Jackson, S., Pearson, N., O'Reilly, S.Y., Xu, X., Zhou, X., 2002. Zircon chemistry and magma mixing, SE China: in-situ analysis of Hf isotopes, Tonglu and Pingtan igneous complexes. Lithos 61, 237–269.
Griffin, W.L., Belousova, E.A., Shee, S.R., Pearson, N.J., O'Reilly, S.Y., 2004. Archean crustal evolution in the northern Yilgarn Craton: U–Pb and Hf isotope evidence from detrital zircons. Precambrian Res. 131, 231–282.
Hanchar, J.M., Van Westrenen, W., 2007. Rare earth element behavior in zircon–melt systems. Elements 3, 37–42.
Hawkesworth, C., Kemp, A., 2006. Using hafnium and oxygen isotopes in zircons to unravel the record of crustal evolution. Chem. Geol. 226, 144–162.
Hoskin, P., Black, L., 2000. Metamorphic zircon formation by solid–state recrystallization of protolith igneous zircon. J. Metamorph. Geol. 18, 423–439.
Hou, K.J., Li, Y.H., Zou, T.R., Qu, X.M., Shi, Y.R., Xie, G.Q., 2007. Laser ablation-MC-ICP-MS technique for Hf isotope microanalysis of zircon and its geological applications. Acta Pet. Sin. 23, 2595–2604 (in Chinese with English abstract).
Hou, K.J., Li, Y.H., Tian, Y.R., 2009. In situ U–Pb zircon dating using laser ablation-multi-ion counting-ICP-MS. Mineral Deposits 28, 481–492 (in Chinese with English abstract).
Hou, Z.Q., Pan, X.F., Li, Q.Y., Yang, Z.M., Song, Y.C., 2013. The giant Dexing porphyry Cu–Mo–Au deposit in east China: product of melting of juvenile lower crust in an intracontinental setting. Mineral. Deposita 48, 1019–1045.
Hou, Z.Q., Duan, L.F., Lu, Y.J., Zheng, Y.C., Zhu, D.C., Yang, Z.M., Yang, Z.S., Wang, B.D., Pei, Y.R., Zhao, Z.D., McCuaig, T.C., 2015a. Lithospheric architecture of the Lhasa Terrane and its control on ore deposits in the Himalayan-Tibetan orogen. Econ. Geol. 110, 1541–1575.
Hou, Z.Q., Yang, Z.M., Lu, Y.J., Kemp, A., Zheng, Y.C., Li, Q.Y., Tang, J.X., Yang, Z.M., Duan, L.F., 2015b. A genetic linkage between subduction- and collision-related porphyry Cu deposits in continental collision zones. Geology 43, 247–250.
Hua, R.M., Mao, J.W., 1999. A preliminary discussion on the Mesozoic metallogenic explosion in East China. Mineral Deposits 18, 300–307 (in Chinese with English abstract).
Hua, R.M., Chen, P.R., Zhang, W.L., Yao, J.M., Lin, J.F., Zhang, Z.S., Guo, C.Y., 2005. Metallogeneses and their geodynamic settings related to Mesozoic granitoids in the Nanling range. Geol. J. China Univ. 11, 291–304 (in Chinese with English abstract).
Hua, R.M., Li, G.L., Zhang, W.L., Hu, D.Q., Chen, P.R., Chen, W.F., Wang, X.D., 2010. A tentative discussion on differences between large-scale tungsten and tin mineralization in South China. Mineral Deposits 29, 9–23 (in Chinese with English abstract).
Huang, H.Q., Li, X.H., Li, X.W., Li, Z.X., 2011. Formation of high $\delta^{18}O$ fayalite-bearing A-type granite by high temperature melting of granulitic metasedimentary rocks, southern China. Geology 39, 903–906.
Huang, J.C., Peng, J.T., Yang, J.H., Zhang, B.L., Xu, C.X., 2015. Precise zircon U–Pb and molybdenite Re–Os dating of the Shuikoushan granodiorite-related Pb–Zn mineralization, southern Hunan, South China. Ore Geol. Rev. 71, 305–317.
Irber, W., 1999. The lanthanide tetrad effect and its correlation with K/Rb, Eu/Eu*, Sr/Eu, Y/Ho, and Zr/Hf of evolving peraluminous granite suites. Geochim. Cosmochim. Acta 63, 489–508.
Jahn, B.M., Wu, F.Y., Capdevila, R., Martineau, F., Wang, Y.X., 2001. Highly evolved juvenile granites with tetrad REE patterns: the Woduhe and Baerzhe granites from the Great Xing'an Mountains in NE China. Lithos 59, 171–198.
Jiang, Y.H., Jiang, S.Y., Dai, B.Z., Liao, S.Y., Zhao, K.D., Ling, H.F., 2009. Middle to late Jurassic felsic and mafic magmatism in southern Hunan province, southeast China: implications for a continental arc to rifting. Lithos 107, 185–204.
Kelley, K.A., Cottrell, E., 2009. Water and the oxidation state of subduction zone magmas. Science 325, 605–607.
Li, F.S., Kang, R.H., Hu, X.Y., Ma, W.L., Huang, X.H., Zeng, Y.H., Tang, J.B., Zhu, X., Qing, Z.W., Zhang, J., He, L.B., 2012. Geological characteristics and ore-search prospect of the Weijia tungsten deposit in Nanling region. Geol. China 39, 445–457 (in Chinese with English abstract).
Li, X.H., Chung, S.L., Zhou, H., Lo, C.H., Liu, Y., Chen, C.H., 2004. Jurassic intraplate magmatism in southern Hunan–eastern Guangxi: $^{40}Ar/^{39}Ar$ dating, geochemistry, Sr–Nd isotopes and implications for the tectonic evolution of SE China. Geol. Soc. Lond. Spec. Publ. 226, 193–215.
Li, X.H., Li, Z.X., 2007. Formation of the 1300-km-wide intracontinental orogen and postorogenic magmatic province in Mesozoic South China: a flat-slab subduction model. Geology 35, 179–182.
Li, X.H., Li, Z.X., Li, W.X., Liu, Y., Yuan, C., Wei, G., Qi, C., 2007a. U–Pb zircon, geochemical and Sr–Nd–Hf isotopic constraints on age and origin of Jurassic I- and A-type granites from central Guangdong, SE China: a major igneous event in response to foundering of a subducted flat-slab? Lithos 96, 186–204.
Li, X.H., Li, W.X., Li, Z.X., 2007b. On the genetic classification and tectonic implications of the Early Yanshanian granitoids in the Nanling Range, South China. Chin. Sci. Bull. 52, 1873–1885.
Li, Z.X., Li, X.H., Zhou, H., Kinny, P.D., 2002. Grenvillian continental collision in south China: new SHRIMP U–Pb zircon results and implications for the configuration of Rodinia. Geology 30, 163–166.
Linnen, R., Cuney, M., 2005. Granite-related rare-element deposits and experimental constraints on Ta–Nb–W–Sn–Zr–Hf mineralization. In: Linnen, R.L., Samson, I.M. (Eds.), Rare-element Geochemistry and Mineral Deposits, in Proceedings Geological Association of Canada, GAC, Short Course.
Liu, S.W., Pan, Y.M., Xie, Q.L., Zhang, J., Li, Q.G., 2004. Archean geodynamics in the Central Zone, North China craton: constraints from geochemistry of two contrasting series of granitoids in the Fuping and Wutaishan complexes. Precambrian Res. 130, 229–249.
Liu, S.W., Pan, Y.M., Xie, Q.L., Zhang, J., Li, Q.G., 2005. Geochemistry of the Paleoproterozoic Nanying granitic gneisses in the Fuping complex: implications for the tectonic evolution of the Central zone, North China Craton. J. Asian Earth Sci. 24, 643–658.
Liu, Y.S., Hu, Z.C., Gao, S., Günther, D., Xu, J., Gao, C.G., Chen, H.H., 2008. In situ analysis of major and trace elements of anhydrous minerals by LA-ICP-MS without applying an internal standard. Chem. Geol. 257, 34–43.
Liu, Y., Xiao, Q.H., Geng, S.F., Wang, X.X., Chen, B.H., 2010. Magmatic mingling origin of adamellite: zircon U–Pb dating and Hf isotopes evidence of microgranular dioritic enclaves and host rocks from Yangtianhu adamellite of Qitianling. South China. Geol. China 37, 1081–1091 (in Chinese with English abstract).
Lu, H.Z., Liu, Y., Wang, C., Xu, Y., Li, H., 2003. Mineralization and fluid inclusion study of the Shizhuyuan W–Sn–Bi–Mo–F skarn deposit, Hunan Province, China. Econ. Geol. 98, 955–974.
Lu, Y.F., Ma, L.Y., Qu, W.J., Mei, Y.P., Chen, X.Q., 2006. U–Pb and Re–Os isotope geochronology of Baoshan Cu–Mo polymetallic ore deposit in Hunan province. Acta Pet. Sin. 22, 2483–2492 (in Chinese with English abstract).
Luck, J.M., Allègre, C.J., 1982. The study of molybdenites through the ^{187}Re–^{187}Os chronometer. Earth Planet. Sci. Lett. 61, 291–296.
Ludwig, K.R., 2001. User's manual for isoplot/ex, v2.49, a geochronological toolkit for Microsoft Excel. Geochronological Center Special Publication, No, la, pp. 1–58.
Ludwig, K.R., 2003. User's Manual for Isoplot/Ex. Version 3.00: a geochronological toolkit for Microsoft Excel. Berkeley Geochronology Center Special Publication, Berkeley, pp. 1–70.

Ma, L.Y., Lu, Y.F., Mei, Y.P., Chen, X.Q., 2006. Zircon SHRIMP U–Pb dating of granodiorite from Shuikoushan ore-field, Hunan province and its geological significance. Acta Pet. Sin. 22, 2475–2482 (in Chinese with English abstract).

Mao, J.W., Li, H.Y., 1995. Evolution of the Qianlishan granite stock and its relation to the Shizhuyuan polymetallic tungsten deposit. Int. Geol. Rev. 37, 63–80.

Mao, J.W., Li, H.Y., Shimazaki, H., Raimbault, L., Guy, B., 1996. Geology and metallogeny of the Shizhuyuan skarn-greisen deposit, Hunan Province, China. Int. Geol. Rev. 38, 1020–1039.

Mao, J.W., Hua, R.M., Li, X.B., 1999a. A preliminary study of large-scale metallogenesis and large clusters of mineral deposits. Mineral Deposits 18, 291–299 (in Chinese with English abstract).

Mao, J.W., Zhang, Z.C., Zhang, Z.H., Du, A.D., 1999b. Re–Os isotopic dating of molybdenites in the Xiaoliugou W–(Mo) deposit in the northern Qilian Mountains and its geological significances. Geochim. Cosmochim. Acta 63 (1845–1818).

Mao, J.W., Li, X.F., Lehmann, B., Chen, W., Lan, X.M., Wei, S.L., 2004. ^{40}Ar–^{39}Ar dating of tin ores and related granite in Furong tin orefield, Hunan province, and its geodynamic significance. Mineral Deposits 23, 164–175 (in Chinese with English abstract).

Mao, J.W., Wang, Y.T., Lehmann, B., Yu, J.J., Du, A.D., Mei, Y.X., Li, Y.F., Zang, W.S., Stein, H.J., Zhou, T., 2006. Molybdenite Re–Os and albite ^{40}Ar/^{39}Ar dating of Cu–Au–Mo and magnetite porphyry systems in the Yangtze River valley and metallogenic implications. Ore Geol. Rev. 29, 307–324.

Mao, J.W., Xie, G.Q., Guo, C.L., Yuan, S.D., Chen, Y.B., Chen, Y.C., 2008. Spatial-temporal distribution of Mesozoic ore deposits in South China and their metallogenic settings. Geol. J. China Univ. 14, 510–526 (in Chinese with English abstract).

Mao, J.W., Zhang, J.D., Guo, C.L., 2010. Porphyry Cu, epithermal Ag–Pb–Zn, distal hydrothermal Au deposits: a new model of mineral deposit-taking the Dexing area as an example. J. Earth Sci. Environ. 32, 1–14 (in Chinese with English abstract).

Mao, J.W., Chen, M.H., Yuan, S.D., Guo, C.L., 2011a. Geological characteristics of the Qinhang (or Shihang) metallogenic belt in South China and spatial-temporal distribution regularity of mineral deposits. Acta Geol. Sin. 85, 636–658 (in Chinese with English abstract).

Mao, J.W., Pirajno, F., Cook, N., 2011b. Mesozoic metallogeny in East China and corresponding geodynamic settings – an introduction to the special issue. Ore Geol. Rev. 43, 1–7.

Mao, J.W., Zhang, J.D., Pirajno, F., Ishiyama, D., Su, H.M., Guo, C.L., Chen, Y.C., 2011c. Porphyry Cu–Au–Mo–epithermal Ag–Pb–Zn–distal hydrothermal Au deposits in the Dexing area, Jiangxi province, East China—a linked ore system. Ore Geol. Rev. 43, 203–216.

Mao, J.W., Cheng, Y.B., Chen, M.H., Franco, P., 2013. Major types and time–space distribution of Mesozoic ore deposits in South China and their geodynamic settings. Mineral. Deposita 48, 267–294.

Mao, Z.H., Liu, J.J., Mao, J.W., Deng, J., Zhang, F., Meng, X.Y., Xiong, B.K., Xiang, X.K., Luo, X.H., 2014. Geochronology and geochemistry of granitoids related to the giant Dahutang tungsten deposit, middle Yangtze River region, China: implications for petrogenesis, geodynamic setting, and mineralization. Gondwana Res. 28, 816–836.

Maniar, P.D., Piccoli, P.M., 1989. Tectonic discrimination of granitoids. Geol. Soc. Am. Bull. 101, 635–643.

Maruyama, S., Isozaki, Y., Kimura, G., Terabayashi, M., 1997. Paleogeographic maps of the Japanese Islands: plate tectonic synthesis from 750 Ma to the present. Island Arc 6, 121–142.

Masuda, A., Kawakami, O., Dohmoto, Y., Takenaka, T., 1987. Lanthanide tetrad effects in nature: Two mutually opposite types, W and M. Geochem. J. 21, 119–124.

McLennan, S.M., 1994. Rare earth element geochemistry and the "tetrad" effect. Geochim. Cosmochim. Acta 58, 2025–2033.

Mi, J.R., Yuan, S.D., Yuan, Y.B., Xuan, Y.S., 2014. Mineral chemistry of biotites in Baoshan granodiorite porphyry, southern Hunan Province: implications for petrogenesis and mineralization. Mineral Deposits 33, 1357–1365 (in Chinese with English abstract).

Middlemost, E.A., 1994. Naming materials in the magma/igneous rock system. Earth Sci. Rev. 37, 215–224.

Miller, C.F., McDowell, S.M., Mapes, R.W., 2003. Hot and cold granites? Implications of zircon saturation temperatures and preservation of inheritance. Geology 31, 529–532.

Monecke, T., Kempe, U., Monecke, J., Sala, M., Wolf, D., 2002. Tetrad effect in rare earth element distribution patterns: a method of quantification with application to rock and mineral samples from granite-related rare metal deposits. Geochim. Cosmochim. Acta 66, 1185–1196.

Mungall, J.E., 2002. Roasting the mantle: slab melting and the genesis of major Au and Au-rich Cu deposits. Geology 30, 915–918.

Peng, J.T., Hu, R.Z., Bi, X.W., Dai, T.M., Li, Z.L., Li, X.M., Shuang, Y., Yuan, S.D., Liu, S.R., 2007. ^{40}Ar/^{39}Ar isotopic dating of tin mineralization in Furong deposit of Hunan Province and its geological significance. Mineral Deposits 26, 237–248 (in Chinese with English abstract).

Peng, J.T., Hu, R.Z., Yuan, S.D., Bi, X.W., Shen, N.P., 2008. The time ranges of granitoid Emplacement and related nonferrous metallic mineralization in southern Hunan. Geol. Rev. 54, 617–625 (in Chinese with English abstract).

Qiu, J.T., Yu, X.Q., Santosh, M., Zhang, D.H., Chen, S.Q., Li, P.J., 2013. Geochronology and magmatic oxygen fugacity of the Tongcun molybdenum deposit, northwest Zhejiang, SE China. Mineral. Deposita 48, 545–556.

Quan, T.J., Wang, G., Zhong, J.L., Fei, L.D., Kong, H., Liu, S.J., Zhao, Z.Q., Guo, B.Y., 2013. Petrogenesis of granodiorites in Tongshanling deposit of Hunan province: constraints from petrogeochemistry, zircon U–Pb chronology and Hf isotope. Mineral. Petrol. 33, 43–52 (in Chinese with English abstract).

Rapp, P.R., Watson, E.B., 1995. Dehydration melting of metabasalt at 8–32 kbar: implications for continental growth and crust-mantle recycling. J. Petrol. 36, 891–931.

Richards, J.P., Boyce, A.J., Pringle, M.S., 2001. Geologic evolution of the Escondida area, northern Chile: a model for spatial and temporal localization of porphyry Cu mineralization. Econ. Geol. 96, 271–305.

Rollinson, H.R., 1993. Using Geochemical Data: Evaluation, Presentation, Interpretation. Longman Scientific and Technical, New York, pp. 1–352.

Selby, D., Creaser, R.A., 2004. Macroscale NTIMS and microscale LA-MC-ICP-MS Re–Os isotopic analysis of molybdenite: testing spatial restrictions for reliable Re–Os age determinations, and implications for the decoupling of Re and Os within molybdenite. Geochim. Cosmochim. Acta 68, 3897–3908.

Shu, L.S., Yu, J.H., Jia, D., Wang, B., Shen, W.Z., Zhang, Y.Q., 2008. Early Paleozoic orogenic belt in the eastern segment of South China. Geol. Bull. China 27, 1581–1593.

Sillitoe, R.H., 2010. Porphyry copper systems. Econ. Geol. 105, 3–41.

Smoliar, M.I., Walker, R.J., Morgan, J.W., 1996. Re–Os ages of group IIA, IIIA, IVA, and VIB iron meteorites. Science 271, 1099–1102.

Söderlund, U., Patchett, P.J., Vervoort, J.D., Isachsen, C.E., 2004. The ^{176}Lu decay constant determined by Lu–Hf and U–Pb isotope systematics of Precambrian mafic intrusions. Earth Planet. Sci. Lett. 219, 311–324.

Stein, H.J., Scherstén, A., Hannah, J.L., Markey, R., 2003. Subgrain-scale decoupling of Re and ^{187}Os and assessment of laser ablation ICP-MS spot dating in molybdenite. Geochim. Cosmochim. Acta 92, 827–835.

Štemprok, M., 1990. Solubility of tin, tungsten and molybdenum oxides in felsic magmas. Mineral. Deposita 25, 205–212.

Sun, S.S., McDonough, W., 1989. Chemical and isotopic systematics of oceanic basalts: implications for mantle composition and processes. Geol. Soc. Lond. Spec. Publ. 42, 313–345.

Sun, W.D., Liang, H.Y., Ling, M.X., Zhan, M.Z., Ding, X., Zhang, H., Yang, X.Y., Li, Y.I., Ireland, T.R., Wei, Q.R., 2013. The link between reduced porphyry copper deposits and oxidized magmas. Geochim. Cosmochim. Acta 103, 263–275.

Wang, R., Richards, J.P., Hou, Z.Q., Yang, Z.M., DuFrane, S.A., 2014. Increased magmatic water content—the key to Oligo-Miocene porphyry Cu–Mo ± Au formation in the Eastern Gangdese Belt, Tibet. Econ. Geol. 109, 1315–1339.

Wang, R., Richards, J.P., Zhou, L.M., Hou, Z.Q., Stern, R.A., Creaser, R.A., Zhu, J.J., 2015. The role of Indian and Tibetan lithosphere in spatial distribution of Cenozoic magmatism and porphyry Cu–Mo deposits in the Gangdese belt, southern Tibet. Earth Sci. Rev. 150, 68–94.

Wang, X., Griffin, W.L., Wang, Z.C., Zhou, X.M., 2003b. Hf isotope composition of zircons and implication for the petrogenesis of Yajiangqiao granite, Hunan Province, China. Chin. Sci. Bull. 48, 995–998.

Wang, Y.J., Fan, W.M., Guo, F., Li, H.M., Liang, X.Q., 2001. U–Pb dating of Mesozoic granodioritic intrusions in southeastern Hunan Province and its petrogenetic implication. Sci. China Ser. D 45, 271–280 (in Chinese with English abstract).

Wang, Y.J., Fan, W.M., Guo, F., 2003a. Geochemistry of early Mesozoic potassium-rich diorites-granodiorites in southeastern Hunan Province, South China: petrogenesis and tectonic implications. Geochem. J. 37, 427–448.

Watson, E.B., Harrison, T.M., 1983. Zircon saturation revisited: temperature and composition effects in a variety of crustal magma types. Earth Planet. Sci. Lett. 64, 295–304.

Wei, D.F., Bao, Z.Y., Fu, J.M., 2007. Geochemical characteristics and zircon SHRIMP U–Pb dating of the Tongshanling granite in Hunan province, South China. Geotecton. Metallog. 31, 482–489 (in Chinese with English abstract).

Wood, S.A., Samson, I.M., 2000. The hydrothermal geochemistry of tungsten in granitoid environments: I. Relative solubilities of ferberite and scheelite as a function of T, P, pH, and mNaCl. Econ. Geol. 95, 143–182.

Wu, F.Y., Jahn, B.M., Wilde, S.A., Lo, C.H., Yui, T.F., Lin, Q., Ge, W.C., Sun, D.Y., 2003. Highly fractionated I-type granites in NE China (I): geochronology and petrogenesis. Lithos 66, 241–273.

Xie, Y.C., Lu, J.J., Ma, D.S., Zhang, R.Q., Gao, J.F., Yao, Y., 2013. Origin of granodiorite porphyry and mafic microgranular enclave in the Baoshan Pb–Zn polymetallic deposit, southern Hunan Province: zircon U–Pb chronological, geochemical and Sr–Nd–Hf isotopic constraints. Acta Pet. Sin. 29, 4186–4214 (in Chinese with English abstract).

Xuan, Y.S., Yuan, S.D., Yuan, Y.B., Mi, J.R., 2014. Zircon U–Pb age, geochemistry and petrogenesis of Jianfengling pluton in southern Hunan Province. Mineral Deposits 33, 1379–1390 (in Chinese with English abstract).

Yao, J.L., Shu, L.S., Santosh, M., Li, J.Y., 2013. Geochronology and Hf isotope of detrital zircons from Precambrian sequences in the eastern Jiangnan Orogen: constraining the assembly of Yangtze and Cathaysia Blocks in South China. J. Asia Earth Sci. 74, 225–243.

Yao, J.M., Hua, R.M., Qu, W.J., Qi, H.W., Lin, J.F., Du, A.D., 2007. Re–Os isotope dating of molybdenites in the Huangshaping Pb–Zn–W–Mo polymetallic deposit, Hunan Province, South China and its geological significance. Sci. China Ser. D 50, 519–526 (in Chinese with English abstract).

Yang, C., Shen, Z.J., Kuang, W.L., Zhang, W.H., 2012. The geological features and minerogenetic mechanism of tungsten–polymetallic deposits in Tongshanling area, southwestern Hunan: taking Xianglinpu deposit as an example. Contrib. Geol. Min. Resour. Res. 27, 156–161 (in Chinese with English abstract).

Yang, J.H., Wu, F.Y., Wilde, S.A., Xie, L.W., Yang, Y.H., Liu, X.M., 2007. Tracing magma mixing in granite genesis: in situ U–Pb dating and Hf-isotope analysis of zircons. Contrib. Mineral. Petrol. 153, 177–190.

Yuan, S.D., Peng, J.T., Shen, N.P., Hu, R.Z., Dai, T.M., 2007. ^{40}Ar–^{39}Ar dating of the Xianghualing Sn–polymetallic orefield in southern Hunan, China and its geological implication. Acta Geol. Sin. 81, 278–286.

Yuan, S.D., Peng, J.T., Hu, R.Z., Bi, X.W, Qi, L., Li, Z.L., Li, X.M, Shuang, Y., 2008a. Characteristics of rare-earth elements (REE), strontium and neodymium isotopes in hydrothermal fluorites from the Bailashui tin deposit in the Furong ore field, southern Hunan Province, China. Chin. J. Geochem. 27, 342–350.

Yuan, S.D., Peng, J.T., Hu, R.Z., Li, H.M., Shen, N.P., Zhang, D.L., 2008b. A precise U–Pb age on cassiterite from the Xianghualing tin-polymetallic deposit (Hunan, South China). Mineral. Deposita 43, 375–382.

Yuan, S.D., Peng, J.T., Li, X.Q., Peng, Q.L., Fu, Y.Z., Shen, N.P., Zhang, D.L., 2008c. Carbon, oxygen and strontium isotope geochemistry of calcites from the Xianghualing tin–polymetallic deposit, Hunan province. Acta Geol. Sin. 82, 1522–1530 (in Chinese with English abstract).

Yuan, S.D., Peng, J.T., Hao, S., Li, H.M., Geng, J.Z., Zhang, D.L., 2011. In situ LA-MC-ICP-MS and ID–TIMS U–Pb geochronology of cassiterite in the giant Furong tin deposit, Hunan Province, South China: new constraints on the timing of tin–polymetallic mineralization. Ore Geol. Rev. 43, 235–242.

Yuan, S.D., Liu, X.F., Wang, X.D., Wu, S.H., Yuan, Y.B., Li, X.K., Wang, T.Z., 2012a. Geological characteristics and ^{40}Ar–^{39}Ar geochronology of the Hongqiling tin deposit in southern Hunan Province. Acta Petrol. Sin. 28, 3787–3797 (in Chinese with English abstract).

Yuan, S.D., Zhang, D.L., Shuang, Y., Du, A.D., Qu, W.J., 2012b. Re–Os dating of molybdenite from the Xintianling giant tungsten–molybdenum deposit in southern Hunan Province, China and its geological implications. Acta Petrol. Sin. 28, 27–38 (in Chinese with English abstract).

Yuan, Y.B., Yuan, S.D., Chen, C.J., Huo, R., 2014. Zircon U–Pb ages and Hf isotopes of the granitoids in the Huangshaping mining area and their geological significance. Acta Petrol. Sin. 30, 64–78 (in Chinese with English abstract).

Zhao, K.D., Jiang, S.Y., Zhu, J.C., Li, L., Dai, B.Z., Jiang, Y.H., Ling, H.F., 2009. Hf isotopic composition of zircons from the Huashan-Guposhan intrusive complex and their mafic enclaves in northeastern Guangxi: implication for petrogenesis. Chin. Sci. Bull. 54, 3716–3725 (in Chinese with English abstract).

Zhao, K.D., Jiang, S.Y., Yang, S.Y., Dai, B.Z., Lu, J.J., 2012. Mineral chemistry, trace elements and Sr–Nd–Hf isotope geochemistry and petrogenesis of Cailing and Furong granites and mafic enclaves from the Qitianling batholith in the Shi-Hang zone, South China. Gondwana Res. 22, 310–324.

Zhao, Z.H., Xiong, X.L., Han, X.D., Wang, Y.X., Wang, Q., Bao, Z.W., Borming, J., 2002. Controls on the REE tetrad effect in granites: evidence from the Qianlishan and Baerzhe Granites, China. Geochem. J. 36, 527–543.

Zhao, P.L., Yuan, S.D., Yuan, Y.B., 2016. Zircon LA–MC–ICP–MS U–Pb dating of the Xianglinpu granites from the Weijia tungsten deposit in southern Hunan Province and its implications for the Late Jurassic tungsten metallogenesis in the westernmost Nanling W–Sn metallogenic belt. Geol. China 43, 120–131 (in Chinese with English abstract).

Zhang, C.L., Santosh, M., Zou, H.B., Li, H.K., Huang, W.C., 2013b. The Fuchuan ophiolite in Jiangnan Orogen: geochemistry, zircon U–Pb geochronology, Hf isotope and implications for the Neoproterozoic assembly of South China. Lithos 179, 263–274.

Zhang, H., Ling, M.X., Liu, Y.L., Tu, X.L., Wang, F.Y., Li, C.Y., Liang, H.Y., Yang, X.Y., Arndt, N.T., Sun, W.D., 2013a. High oxygen fugacity and slab melting linked to Cu mineralization: evidence from Dexing porphyry copper deposits, Southeastern China. J. Geol. 121, 289–305.

Zhong, L.F., Li, J., Peng, T.P., Xia, B., Liu, L.W., 2013. Zircon U–Pb geochronology and Sr–Nd–Hf isotopic compositions of the Yuanzhuding granitoid porphyry within the Shi–Hang Zone, South China: petrogenesis and implications for Cu–Mo mineralization. Lithos 177, 402–415.

Zhou, M.F., Yan, D.P., Kennedy, A.K., Li, Y., Ding, J., 2002. SHRIMP U–Pb zircon geochronological and geochemical evidence for Neoproterozoic arc–magmatism along the western margin of the Yangtze Block, South China. Earth Planet. Sci. Lett. 196, 51–67.

Zhou, X.M., Sun, T., Shen, W.Z., Shu, L.S., Niu, Y.L., 2006. Petrogenesis of Mesozoic granitoids and volcanic rocks in South China: a response to tectonic evolution. Episodes 29, 26.

Zhou, Y.Z., Zeng, C.H., Li, H.Z., An, Y.F., Liang, J., Lv, W.C., Yang, Z.J., He, J.G., Shen, W.J., 2012. Geological evolution and ore–prospecting targets in southern segment of Qinzhou Bay–Hangzhou Bay juncture orogenic belt, southern China. Geol. Bull. China 31, 486–491 (in Chinese with English abstract).

Zhu, J.C., Wang, R.C., Lu, J.J., Zhang, H., Zhang, W.L., Xie, L., Zhang, R.Q., 2011. Fractionation, evolution, petrogenesis and mineralization of Laiziling granite pluton, southern Hunan Province. Geol. J. China Univ. 17, 381–392 (in Chinese with English abstract).

Zuo, C.H., Lu, R., Zhao, Z.X., Xu, Z.W., Lu, J.J., Wang, R.C., Chen, J.Q., 2014. Characterization of element geochemistry, LA–ICP–MS zircon U–Pb age, and Hf isotope of granodiorite in the Shuikoushan deposit, Changning, Hunan Province. Geol. Rev. 60, 811–823 (in Chinese with English abstract).